A Review of Modern Seismic Yield Estimation Techniques and Their Uncertainties

Final Technical Report
Under DOS Contract No 19AQMM19P2238
(30 Sept 2019 – 31 May 2020)

Prepared by:
Vanessa Napoli
Applied Research Associates, Inc

Submitted to
U.S. Department of State
2201 C Street, NW
Washington, DC 20520

31 May 2020

Approved for Public Release; Distribution Unlimited

REPORT DOCUMENTATION PAGE			*Form Approved OMB No. 0704-0188*
Public reporting burden for this collection of information is estimated to average 1 hour per response, including the time for reviewing instructions, searching existing data sources, gathering and maintaining the data needed, and completing and reviewing this collection of information. Send comments regarding this burden estimate or any other aspect of this collection of information, including suggestions for reducing this burden to Department of Defense, Washington Headquarters Services, Directorate for Information Operations and Reports (0704-0188), 1215 Jefferson Davis Highway, Suite 1204, Arlington, VA 22202-4302. Respondents should be aware that notwithstanding any other provision of law, no person shall be subject to any penalty for failing to comply with a collection of information if it does not display a currently valid OMB control number. **PLEASE DO NOT RETURN YOUR FORM TO THE ABOVE ADDRESS.**			
1. REPORT DATE ***(DD-MM-YYYY)*** 05-31-2020	**2. REPORT TYPE** Final Technical Report		**3. DATES COVERED** ***(From - To)*** 30 Sept 2019 – 31 May 2020
4. TITLE AND SUBTITLE A Review of Modern Seismic Yield Estimation Techniques and Their Uncertainties			**5a. CONTRACT NUMBER** 19AQMM19P2238
			5b. GRANT NUMBER
			5c. PROGRAM ELEMENT NUMBER
6. AUTHOR(S) Napoli, Vanessa			**5d. PROJECT NUMBER**
			5e. TASK NUMBER
			5f. WORK UNIT NUMBER
7. PERFORMING ORGANIZATION NAME(S) AND ADDRESS(ES) Applied Research Associates, Inc 181 Bedford St., Suite 1 Lexington, MA 02420			**8. PERFORMING ORGANIZATION REPORT NUMBER** AVC-VTN-20-G01
9. SPONSORING / MONITORING AGENCY NAME(S) AND ADDRESS(ES) Department of State / Arms Control, Verification, and Compliance Bureau Office of Assistant Secretary, HST Room 5888 2201 C Street, NW Washington DC 20520			**10. SPONSOR/MONITOR'S ACRONYM(S)** DOS/AVC
			11. SPONSOR/MONITOR'S REPORT NUMBER(S)
12. DISTRIBUTION / AVAILABILITY STATEMENT UNCLASSIFIED; DISTRIBUTION TO PUBLIC AUTHORIZED			
13. SUPPLEMENTARY NOTES This project was funded by DOS/AVC and issued by DOS/A/AQM through BAA2019-DOC/AVC-0001.			
14. ABSTRACT The data-processing techniques seismologists use to estimate yield have radically improved over the last couple of decades, as has our understanding of seismic energy propagation, which has led to better modeling of source and path effects. Yield estimation has been steadily progressing with techniques that were able to successful discriminate nuclear and chemical explosions from natural seismicity. The seismic monitoring community's grasp on yield estimation changed after The Democratic People's Republic of Korea (DPRK) tested an underground nuclear weapon in 2006 and traditional discrimination methods failed to identify the event. Since 2006, there have been 5 more DRPK nuclear tests, and all 6 of the events have increased uncertainty in modern yield estimation and discrimination techniques as even the most modern estimation methods generate a wide range of yields varying by more than two hundred kilotons in some cases. This report outlines and describe modern yield techniques as they have evolved from the 1988 Office of Technology Assessment while highlighting how certain techniques have improved DPRK yield estimation as well as a specific focus on the causes of these discrepancies in DPRK yield estimates.			
15. SUBJECT TERMS Yield estimation, DPRK nuclear tests, event discrimination, modern yield techniques			
16. SECURITY CLASSIFICATION OF:			**17. LIMITATION OF ABSTRACT**
a. REPORT UNC	**b. ABSTRACT** UNC	**c. THIS PAGE** UNC	
18. NUMBER OF PAGES 46	**19a. NAME OF RESPONSIBLE PERSON** Rongsong Jih, COR		
	19b. TELEPHONE NUMBER ***(include area code)*** 202-647-8126		

Table of Contents

List of Figures

List of Tables

1. Introduction

The data-processing techniques seismologists use to estimate yield have radically improved over the last couple of decades, as has our understanding of seismic energy propagation, which has led to better modeling of source and path effects. Yield estimation has been steadily maturing through the application of techniques that successfully discriminate nuclear and chemical explosions from natural seismicity. Various methods evolved to incorporate multiple seismic phases for reducing uncertainty, and as seismic sensors were deployed globally, the ability to measure smaller events at regional and local distances increased.

Even with the continual progress that has been made in yield estimation, multiple complex sources of uncertainty remain. For instance, seismic yield estimates rely on remotely observed signals whose strength derives from the energy radiated away from the source region minus the energy near the source that is absorbed through rock vaporization, melting, cracking and heating. Accurate measurements of radiated energy versus absorbed energy will always be difficult to achieve. Another troublesome source of uncertainty arises from seismic magnitude scales, which vary between agencies, time periods, station choice, and other factors. To achieve the full potential of seismological methods to estimate yield accurately, the magnitudes used in formulas relating magnitude and yield must be carefully examined. Throughout this report, we address how different uncertainties are accounted for in modern yield techniques and highlight where future research should focus.

The seismic monitoring community's grasp on yield estimation changed after the Democratic People's Republic of Korea (DPRK) tested an underground nuclear weapon in 2006, when traditional discrimination methods failed to identify the event. The DPRK conducted five more shots after 2006, and the six events have revealed the endemic uncertainties in yield estimation and discrimination, as even the most modern estimation methods generate a wide range of yields that vary by more than two hundred kilotons (Pasyanos and Myers, 2018). Since 2006, improving yield estimates for the DPRK tests has been a major research objective, with the expectation that advances on those tests will lead to improved yield estimation globally. Research has focused around developing techniques to constrain emplacement conditions, measuring effects from topography, using satellite imagery to quantity ground displacement, and measuring seismo-acoustic energy partitioning to constrain depth-of-burial (DOB).

In this report, we describe modern yield techniques that have evolved following the 1988 Office of Technology Assessment (OTA). Because the DPRK tests drove much of the improvement in seismic yield estimation over the last 15 years, we begin by describing the difficulties monitoring seismologists found when analyzing the DPRK recordings. Then we focus on six major categories of yield techniques including methods that use (1) body waves, (2) surface waves, (3) ground displacement measurements, (4) source spectra, (5) seismic moment and moment tensor inversion, and (6) multi-technology methods that include seismo-acoustic measurements. In each section, we review the various yield-estimation techniques, and highlight how certain estimation techniques have improved DPRK yield estimation and focus on the causes of discrepancies in DPRK yield estimates.

2. Background

The *OTA* (1988) stated that seismic yield estimation was limited to teleseismic distances (defined as > 2000 km), especially for Soviet yields, due to the lack of seismic stations close enough to measure signals in areas of interest for treaty monitoring. Since 1988, the numbers of seismic stations have significantly increased in areas of interest, to include the International Monitoring System (IMS), an expanded Global Seismic Network (GSN), and countless seismic networks deployed by countries, government agencies, and universities. We now have seismic recordings at local, regional, and teleseismic distances for regions of interest, which in turn has allowed yield estimation to extend to events recorded at local and regional distances. At closer distances, we can measure the yield of smaller events (m_b < 4), which is of strong interest to the monitoring community. In this report we review both teleseismic yield methods and newer techniques applied to smaller events observed at regional and local distances. Our study analyzes the progress in yield estimation from 1988 to the present day and identifies the sources of remaining uncertainties that must be addressed in future research efforts.

2.1. Background on DPRK Nuclear Tests

The DPRK conducted six underground nuclear tests at the Punggye-ri test site between 2006-2017. At approximately 8.5 minutes after DPRK6, a second seismic event occurred at the test site that many researchers speculate was a collapse. In the following weeks, several small seismic events were reported near the test site that have become a topic of interest in the monitoring community.

The absolute and relative locations of the six DPRK tests have been calculated in many studies (Murphy et al., 2013; Zhang and Wen, 2013; Zhao et al., 2017; Gibbons et al. 2017). The locations in Table 1 are from Myers et al. (2018) and are relative locations, using DPRK2 as the master event.

Table 1. Information about the six DPRK announced nuclear tests

Event	Date (MM/DD/YYYY)	Latitude*	Longitude	m_b(IDC)	Yield range† (kt)	DOB Range† (m)
DPRK1	10/09/2006	41.29192	129.10907	4.1	0.5-2.0	129-600
DPRK2	05/25/2009	41.29654	129.08298	4.5	1.0-10.5	200-800
DPRK3	02/12/2013	41.29276	129.07851	4.9	7.5-32.5	320-700
DPRK4	01/06/2016	41.29932	129.07662	4.8	2.0-24.4	327-800
DPRK5	09/09/2016	41.29983	129.08157	5.1	3.0-115	476-800
DPRK6	09/03/2017	41.29999	129.07901	6.1	30-300	450-800

DPRK, Democratic People's Republic of Korea; IDC, International Data Centre; DOB, Depth of Burial
*Locations are from Myers et al. (2018)
† Yields and DOB ranges are from all sources in this report

(a) (b)

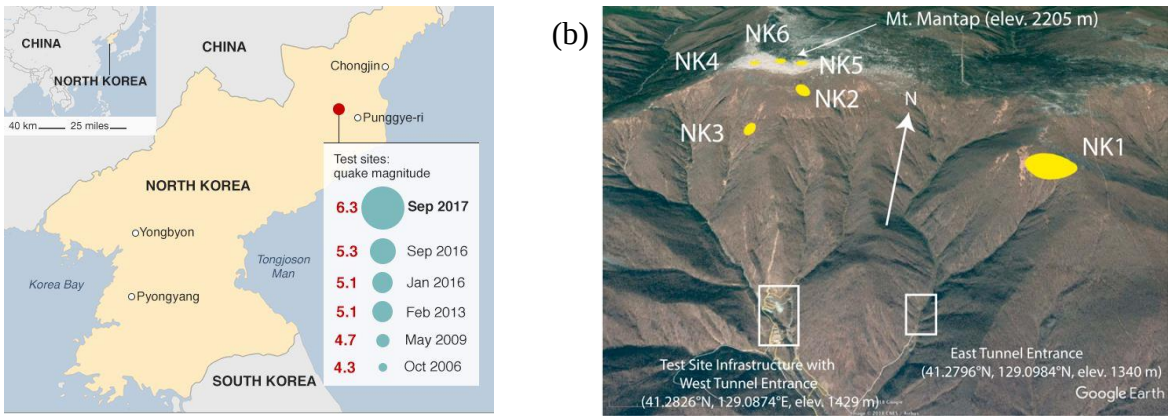

Figure 1. (a) Location of Punggyre-ri Test Site from USGS with m_b(USGS) values listed and (b) the calculated locations of DPRK shots from Voytan et al. (2019). Size of yellow ellipse corresponds to uncertainty in location calculation (95% probability) from Myers et al. (2018).

Yield estimation for the DPRK events must account for more unknowns, such as source geology, topography effects, and emplacement conditions, compared to events at well-studied test sites. The uncertainty introduced into yield techniques because of these unknowns increased the range of yield estimates.

Additionally, the DPRK events had anomalously large *Ms* amplitudes compared to their m_b amplitudes, which caused traditionally stable m_b-*Ms* discrimination methods to improperly identify the DPRK explosions.

Issues of discrimination and yield estimation still can be improved today for the DPRK nuclear tests. This report provides a summary of modern yield estimation techniques, with a focus on the techniques applied to the DPRK tests. In doing this, we have combined modern yield estimates for the six DPRK tests into one concise location, highlighting the assumptions, uncertainties and advantages of each method. Not all methods discussed in this report are applied to the DPRK tests, as the overall objective is to summarize how modern yield techniques have advanced over the last 30 years.

3. Technical Review of Yield Estimation

3.1 Body-wave Measurements

3.1.1 Teleseismic P-wave Estimates

Using teleseismic P-waves to estimate yield has been a long-standing method, since P waves are recorded at far distances even at small magnitudes. Body-wave magnitude, m_b, is defined as:

$$\boldsymbol{m_b = log\left(\frac{A}{T}\right) + B}, \qquad (1)$$

where A is the short-period P-wave amplitude measured in nm, T is the measurement period, and B is a distance-dependent correction term (Murphy, 1981). Teleseismic P waves have simple propagation effects compared to other seismic phases (Chaves et al, 2018); however, to relate m_b

to yield the seismic amplitude must be corrected for non-source related effects (Jih and Wagner, 1991). The complexities can arrive from free-surface reflections from topography (*pP*) and ill-constrained anelastic effects (Chaves et al., 2018). From equation 1, m_b-yield relations are generally defined as:

$$\boldsymbol{m_b = A + B\,log(W)}, \qquad (2)$$

where A and B are empirically derived constants depending on location, and W is the yield in kt (Murphy, 1981, Murphy, 1996; Ringdal et al., 1992). The constants A and B have been derived from explosion data at various test sites of interest. The m_b-yield relationships then account for the specific geologies, average containment depth of explosions, and upper mantle attenuation, and are still used today as reliable yield calculations from m_b.

For example, Murphy (1981) derived the m_b-yield relation at the Nevada Test Site (NTS) to be $m_b = 3.92 + 0.81 \log(W)$ (Figure 1). Murphy (1996) and Ringdal et al. (1992) derived the relation at Semipalatinsk to be $m_b = 4.45 + 0.75 \log(W)$. Bowers et al. (2001) derived a magnitude relation for Novaya Zemlya with the form $m_b = 4.25 + 0.75 \log(W)$.

The stable hard-rock geology of the Punggyre-ri test site is comparable to that of Semipalatinsk or Novaya Zemlya (Kim and Rodgers, 2007; Zhao et al., 2016) and those relations are used more frequently than the NTS relation, which is relevant in more active tectonic regimes. Additional studies such as, Jih et al. (1993), derived various mb scaling formulas for Soviet tests such as m_b(Pa), m_b(Pb), m_b(Pmax), that could also be applicable for scaling at the Punggyre-ri test site.

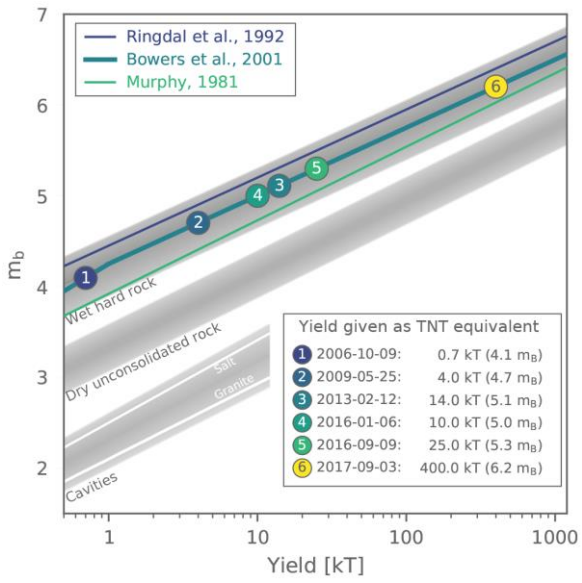

Figure 2**.** Magnitude-yield curves for various geologies with yield estimates for the six DPRK nuclear tests, derived with the listed m_b values using the Bowers et al. (2001) equation: $m_b = 4.25 + 0.75 \log(W)$. Gray shading represents the upper and lower boundaries from the literature for different geologies (from Gaebler et al., 2019). It should be noted the depth effects accounted for in these equations apply to underground nuclear explosions (UNEs) in shafts. Tunnel shots, such as those at Punggyre-ri are generally not at such depths.

These relations assume a fully coupled explosion (120m/kt$^{1/3}$); however, the actual depth-of-burial (DOB) can vary for an underground nuclear test. Patton and Taylor (2011) proposed a correction term based on the scaling relationship derived from body-wave magnitudes from Denny and Johnson (1991):

$$-\mathbf{0.7875}\ \boldsymbol{log}\left(\frac{\boldsymbol{h}}{\mathbf{120}\boldsymbol{Y}^{\frac{\mathbf{1}}{\mathbf{3}}}}\right)\boldsymbol{log}(\boldsymbol{W}). \qquad (3)$$

Because of the effects of a partially buried source on yield estimates, unknown DOB produces a large uncertainty in yield estimation. For the DPRK tests, DOB is unknown; thus, constraining the depth is crucial to correct for effects due to topography and overburden. A study by Voytan et al. (2019) performed waveform equalization of short-period teleseismic P waves to constrain the yield and depth for all six DPRK nuclear tests. Voytan et al. (2019) account for the changing source function and depth phases between pairs of events to constrain yield and depth across multiple events simultaneously (Figure 3). To accomplish this, *P* and *Pn* waves are convolved with the effective source functions from the other event in the pair. A search is done over the effective source function parameters to minimize the waveform difference residual. The result is an intercorrelated waveform that will be similar between the event pairs if yield and depth estimates are accurate from the effective source function.

Figure 3 shows the results for the six DPRK tests, comparing the narrowband 4-Hz yield estimate, W_{4Hz} to the intercorrelation estimate, W_{IC}. The yield estimates from intercorrelation, W_{IC}, produce a yield-calibrated relation of m_b(NEIC)= 0.9 logW_{IC} + 4.13 at the North Korean test site (Voytan et al., 2019). This method greatly reduces uncertainty caused by poorly constrained depth and source function, which is especially useful in North Korea given the many unknowns about emplacement conditions.

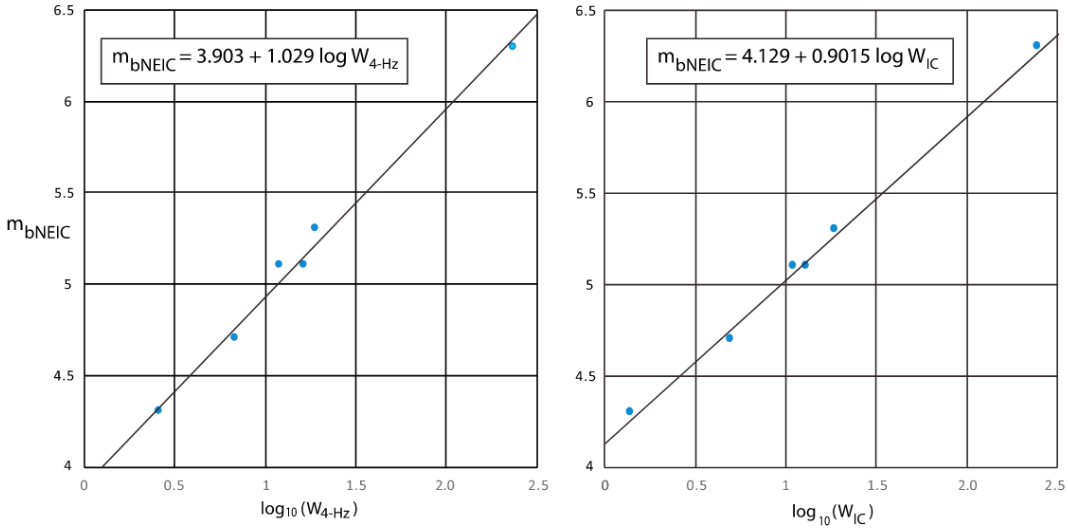

Figure 3. From Voytan et al. (2019). m_b(NEIC) vs yields from W_{4Z} and W_{IC} and the m_b-W linear yield scaling curves for each.

Over the years, many studies have defined m_b-yield regression relations which are effective, but these regressions are specific to the magnitude scale used to derive them (e.g., m_b(NEIC), m_b(ISC),

m_b(IDC)). These regressions are also tied to the global networks used at the time of derivation and rely on having quality data to perform the analysis. As seismic networks have expanded to cover more regions and as station sensitivity to seismic activity has improved over the last couple of decades, m_b-yield relations could also be re-examined to achieve full potential of seismic yield techniques and to take advantage of well-recorded waveforms at regional and local distances.

3.1.2 Regional P-wave Estimates

3.1.2.1 m_b(Pn)

As seismic stations increased in numbers around the globe, seismologists began reliably measuring regional seismic phases. This subsequently improved low-yield event estimation. The traditional m_b(Pn)-yield relationship from Denny et al. (1987) for the Western US is defined as

$$\boldsymbol{m_b(Pn) = log\, A + 2.42\, log\, \Delta - 3.96 + c_i\, log(W)}, \quad (4)$$

where A is the maximum peak-to-peak amplitude measured in nanometers, Δ is the epicenter distance in km, and c_i are station corrections. Vergino and Mensing (1990) extended this work to account for a network-averaged magnitude that was tested on a dataset from NTS with explosions ranging in yield from 1-300 kt. They defined the m_b(*Pn*)-yield as

$$\boldsymbol{m_b(Pn) = A_r + 0.91\, log\, (Y)\ log(W)}, \quad (5)$$

where A_r varies between 3.76 and 3.87 for different areas within NTS. They determined that this relation was valid for any rock type, including dry alluvium.

3.1.2.2 m_b(Lg)

Another body-wave magnitude, m_b(*Lg*), uses scattered high-frequency surface waves known as *Lg* which can help estimated yield of smaller explosions. Nuttli (1973, 1986a) was the first to define a method for calculating yield from the *Lg* phase, using a dataset from NTS, and calibrate it for both water-saturated rock and unsaturated material. *Lg* attenuation must be well calibrated for the propagation paths to reduce uncertainty.

Using the m_b(*Lg*) scale defined in Nuttli (1973), seismic yield can be estimated from the *Lg* phase using the formula

$$\boldsymbol{m_b\,(L_g) = 5.0 + log\left[\frac{A(10km)}{110}\right]}, \quad (6)$$

where A(10km) is the Lg-wave amplitude measured in μm corrected to a distance of 10 km, and the scalar value 110 is a calibration constant that must remain regionally independent for the method to be transportable (Nuttli, 1986).

Given a quadratic assumption and using data from NTS, Nuttli (1986a) defines the m_b(Lg)-yield relation for explosions in water-saturated rock as

$$\boldsymbol{m_b(L_g) = 3.943 + 1.124\, log\, Y - 0.0829(Log\, Y)^2}, \quad (7)$$

and for unsaturated rock as

$$\boldsymbol{m_b(L_g) = 3.869 + 1.110\, log\, Y - 0.146(Log\, Y)^2.} \qquad \textit{(8)}$$

Since $m_b(Lg)$ is stable from site to site compared to other phases, it can be used to estimate the m_b(P) bias across different areas of interest.

An important step in Nuttli's work was the research on the transportability of his method to other areas of interest such as Semipalatinsk (Nuttli, 1986b) and Novaya Zemlya (Nuttli, 1988). Many scientists have extended and built upon Nuttli's method of measuring *Lg* waves to estimate yield. Jih et al. (1994) revised the absolute *Lg* excitation level for Novaya Zemlya explosions from Nuttli's measurements and showed the systematic bias in the *Lg* scale can be removed. Also, multiple studies show that instead of using Nuttli's 3rd-peak amplitude measurement, root-mean-square (RMS) amplitudes can be used as a stable measure of sustained *Lg* ground motion (e.g. Patton 1988; Hansen et al. 1990; Ringdal et al. 1992; Priestley & Patton 1997; Schlittenhardt, 2001; Figure 4). The RMS *Lg* magnitude is based on the log of the RMS-squared amplitudes in the group velocity window centered on *Lg* group velocity (Ringdal, 1983). Priestley and Patton (1997) found no significant difference between *Lg* RMS amplitudes and 3rd-peak amplitudes for central Asian earthquakes and explosions. However, Schlittenhardt (2001) analyzed RMS measurements recorded across two arrays at longer periods and distances for 14 underground nuclear explosions from the eastern Kazakhstan test site and found lower-uncertainty seismic yields results compared to Nuttli (1986b).

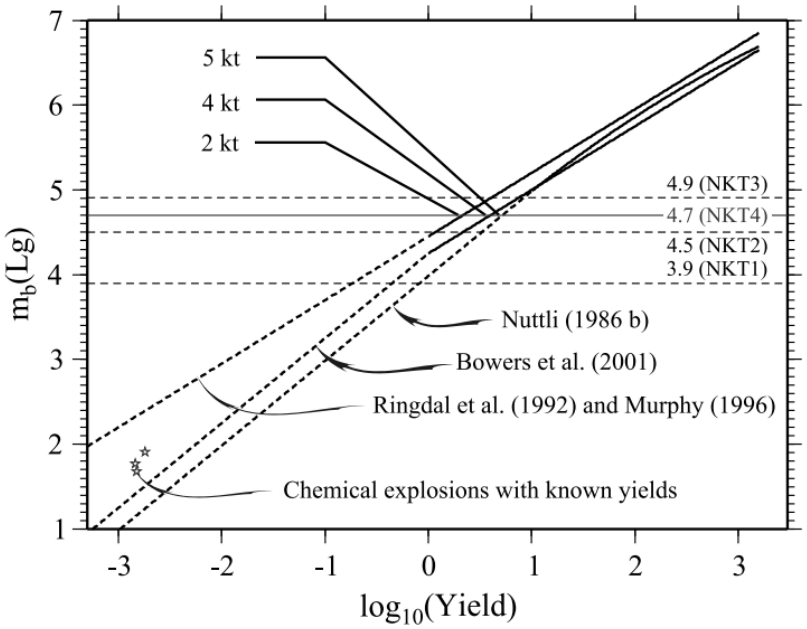

Figure 4. Empirical magnitude–yield relations from Ringdal et al. (1992), Murphy (1996), Bowers et al. (2001), and Nuttli (1986a). Segments supported by observations are illustrated by solid lines, while the dashed lines are extrapolations. The horizontal dashed line

indicates the estimated $m_b(Lg)$ for DPRK1-4. This highlights the variations in m_b(Lg) methods to estimate yield, especially at smaller magnitudes. From Zhao et al. (2016).

Zhang and Wen (2013), applied the depth correction term from Zhao et al. (2012), which was derived using body waves but applicable to Lg waves, since magnitudes derived from *Lg* waves are linear to those from body waves. This resulted in a depth corrected $m_b(Lg)$-Y relation defined as:

$$\boldsymbol{m_b = 1.0125\, log(Y) - 0.7875\, log(h) + 5.887} \qquad (9)$$

Zhang and Wen (2013) combined data from previous tests, seismic data from DPRK3, and current satellite imagery to estimate the yield as 12.2 ± 3.8 kt and the location at 41°17′26.88″N, 129°4′34.68″E with a precision of 94 m. Zhao et al. (2014, 2016, 2017) applied this method to the remaining DPRK tests (results in Table 3).

3.1.3 P/S Discriminants

Various seismic discrimination techniques exist to classify an event as an earthquake, explosion or collapse. While some traditional techniques, e.g., m_b-*Ms*, have had difficulties classifying the DPRK tests (see Section 3.2.3), regional P/S discriminants are still effective (Walter et al., 2018), even though there are still questions as to why explosions generate S waves. This lack of theoretical explanation adds difficulties in generating a predictable explosion S-wave model (Walter et al., 2018). Even with this complexity, P/S ratios can separate the DPRK tests from both tectonic earthquakes and the collapse event after DPRK6 (Kim et al., 2018; Zhao et al., 2018; Walter et al., 2018).

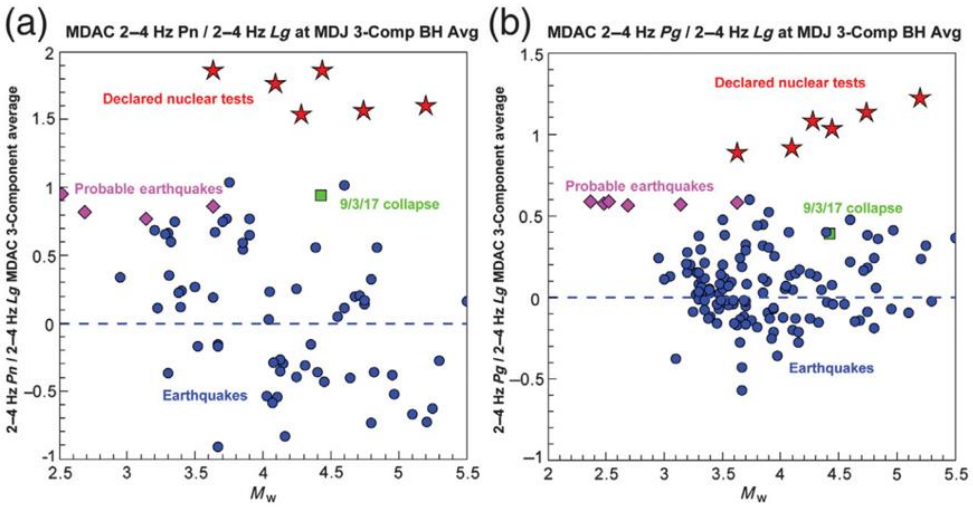

Figure 5. Low/high frequency P/S ratios from Walter et al. (2018) for the DPRK tests, regional earthquakes and the collapse event on 3 Sept 2017.

3.1.4 Estimates Based on P-Coda and Full-waveform Measurements

Research around methods that utilize more of the seismic event record have become more popular as capabilities to process the entire waveform become available. Early versions of these techniques analyzed the amplitude behavior of coda envelopes at single stations. For example, Mayeda and Walter (1996) developed a single-station coda-envelope method that produced more stable magnitude estimates compared to direct P-wave measurement methods. Phillips et al. (2011) and Paysanos et al. (2012) further refined these techniques and applied them to a variety of earthquakes and explosions.

More recently, Yoo (2017) developed a new amplitude measurement tool to improve yield estimates for small underground explosions at local and regional distances. This tool employs an improved hybrid waveform-envelope modeling method and quantifies the uncertainties in the modeling parameters using sophisticated techniques such as tomographic calibration. The Yoo (2017) waveform-envelope modeling technique accounts for both forward and wide-angle scattering in the body-wave code to more accurately capture direct-wave and early coda complexity. Yoo (2019) applied the method to the 6 DPRK nuclear tests (Figures 6).

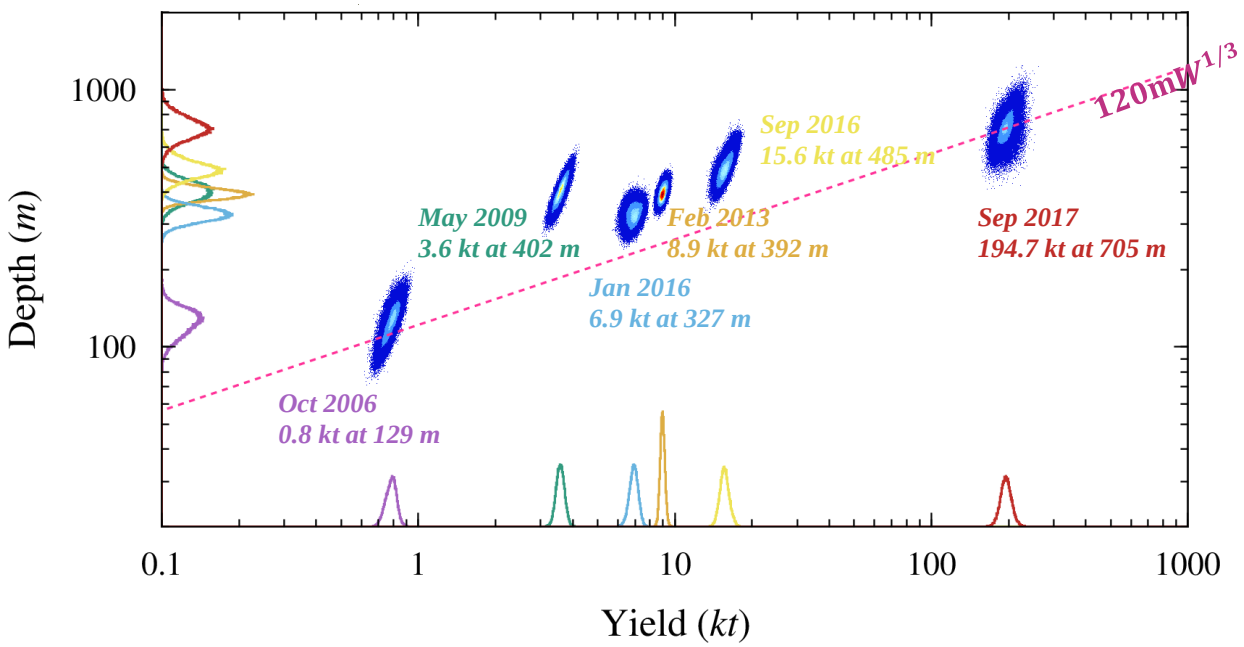

Figure 6. Depth versus yield for the 6 DPRK nuclear tests calculate using Yoo (2017) full-waveform template matching technique. The depth estimates are in good agreement with the estimated depth based on the elevation of the Mt. Mantap and portal entrances. The yield estimates are in good agreement with the estimates of other studies shown in this report (Table 1; Table 3). Each curve on the x and y axes are color coded to their event and represent a 95% confidence interval including uncertainties in measured amplitudes, propagation and site amplification effects. Additional details provided in Yoo (2019).

Table 2 summarizes each method described in this section and includes relevant references, assumptions, formulas, uncertainties and advantages. Table 3 is a summary of published DPRK yield estimates found using each method with Figure 7 visualizing the results in Table 3.

Table 2. Summary of body-wave yield estimation methods, including assumptions, uncertainties and advantages.

Method	References	Assumptions	Formula/Description of Method	Uncertainties	Advantages
Teleseismic P Amplitudes	Murphy (1991); Murphy (1996); Ringdal et al. (1992); Bowers et al. (2001)	Accounts for upper mantle attenuation, depth of containment, and specific geologies in coefficients	NTS: m_b = 3.92 + 0.81 log(W) Semipalatinsk: m_b=4.45 + 0.75 log(W) NZ: m_b=4.25 + 0.75 log(W), where the constants are empirically derived depending on location, and W is yield in kt	site-specific; there is uncertainty in transportability; calibrated for fully-coupled explosions	The Semipalatinsk and Novaya Zemlya m_b-Y relationships have been used for the DPRK shots since they have similar geologies.
Teleseismic P wave stacking	Chaves et al. (2018)	Assumes the Muller-Murphy model is valid; assumes standard granite source parameters and extensive near source damage	broadband P waveforms are stacked in azimuthal windows to average path effects; waveform stacks are modeled using a MM explosion source model; yield is estimated by fitting the waveforms	Uncertainties from ill-constrained t*, topographic effects on pP and scattered coda from irregular surfaces and if incorrectly	No need to calibrate a m_b-yield relationship for the test site, which can be difficult with limited information of parameters such as site-specific coupling effects and poorly constrained attenuation for the region.
Teleseismic P waveform equalization	Voytan et al. (2019)	Assumptions of specific source rock properties that allow for reduction due to weathering, damage zones and rock layering; assumes a specific explosion source model	$m_{b\mathrm{NEIC}}$=0.9 log W_{IC} + 4.13	range of each yield estimate takes into account the fitting over the spread of the uncertainty in t* and the standard deviation of the event average amplitude	Searching over yield and burial depth for both events gives optimal parameters by simultaneous waveform equalization of multiple stations
m_b(Pn)	Vergino and Mensing (1990)	Initial magnitude-yield relationships are developed assuming equal station magnitude variances and no correlations between the station magnitudes.	$m_b(Pn) = A_r + 0.91 \log(Y)$ where A_r varies between 3.76 and 3.87 for different areas within NTS.	Two sources of uncertainty are random measurement variation and the physical variation in the vicinity of the explosion source media, at the test site. When tested at NTS, yield uncertainty was approximately 1.7-1.8, at the 2σ level	They determined that this relation was valid for any rock type, including dry alluvium.
m_b(Lg)	Nuttli (1973); Ringdal (1983); Nuttli (1986a,b)	The frequency dependence of Q for Lg waves was assumed to satisfy the relation from Mitchell (1980): $Q(f) = Q_o f^{\zeta}$, where ζ is constant over the range of frequencies of interest, from 2 to 0.1 Hz.	$m_b(L_g) = 3.943 + 1.124\, log\, Y - 0.0829(Log\, Y)^2$, for saturated rock $m_b(L_g) = 3.869 + 1.110\, log\, Y - 0.146(Log\, Y)^2$, for unsaturated rock	greatest uncertainty is from Q and ζ	$m_b(L_g)$ is stable from site to site compared to other phases

RMS m_b(Lg)	Hansen et al. (1990); Schlittenhardt (2001); Patton and Schlittenhardt (2005)	noise sample was assumed to be stationary and uncorrelated with the *Lg* signal in the analysis window which could lead to over-correcting *Lg* amplitudes by a small amount	$m_b(Lg;rms) = 5.0 + log_{10}\left[\frac{A_{rms}}{C_{rms}}\right]$ defined a new m_b(Lg) RMS magnitude where A_{rms} is the Lg RMS amplitude and C_{rms} is a constant that ties the RMS Lg amplitude to teleseismic m_b	lower-uncertainty seismic yields results compared to Nuttli (1986a) for underground nuclear explosions from the east Kazakh test site	Stable yield measurements even with few stations
Depth corrected m_b(Lg)	Zhang and Wen (2013); Zhao et al. (2012)	Since Lg waves are linear to body waves, apply depth correction term from Zhao et al. (2012) derived using body waves to account for varying DOB	$m_b = 1.0125\log(Y) - 0.7875\log(h) + 5.887,$ where Y is yield in kt and h is DOB in m	The local 3-D structure near the source can cause additional scattering, which would complicate the waveforms and cause errors in the cross-correlations.	Enhanced Nuttli's (1973, 1986) m_b(Lg) formula to be applicable for various DOBs.
Full waveform template matching	Yoo (2017); Yoo (2019)	Method is an extension of the coda-derived source calibration methodology (after Mayeda and Walter, 1996) using multiple-coda type method (Phillips *et al.*, 2011) and a multi-phase amplitude envelope method (Pasyanos *et al.*, 2012)	new hybrid envelope modeling technique that includes multiple forward- and wide-angle-scattering which stabilizes the amplitude measurement. Additionally, Yoo developed a tomographic calibration method using a trans-dimensional Bayesian tomography method to improve source characterization (See Yoo, 2017; Yoo, 2019 for full equation)	estimated uncertainties are included in measured amplitudes, propagation and site amplification effects	Improves yield estimates for small underground explosions at local and regional distances

Table 3. Summary of DPRK nuclear test yield estimates from body-wave measurements.

Source	DPRK1	DPRK2	DPRK3	DPRK4	DPRK5	DPRK6	Description
Murphy (1996) w/ mb(IDC)	0.3 kt m_b(IDC)=4.1	1.2 kt m_b(IDC)=4.5	4.0 kt m_b(IDC)=4.9	2.9 kt m_b(IDC)=4.8	7.3 kt m_b(IDC)=5.1	158.5 kt m_b(IDC)=6.1	m_b=0.75log(W) + 4.45
Murphy (1996) w/ mb(NEIC)	0.6 kt m_b(NEIC)=4.3	2.9 kt m_b(NEIC)=4.8	7.3 kt m_b(NEIC)=5.1	7.3 kt m_b(NEIC)=5.1	13.6 kt m_b(NEIC)=5.3	292.9 kt m_b(NEIC)=6.3	m_b=0.75log(W) + 4.45
mb(NOR) NORSAR (2018)	0.5 kt m_b(NOR)=4.0	1-3 kt m_b(NOR)=4.5	10 kt m_b(NOR)=5.0	5 kt m_b(NOR)=4.8	10-15 kt m_b(NOR)=5.1	200-300 kt m_b(NOR)=6.1	m_b=0.75log(W) + 4.3
mb(BGR) BGR (2018)	0.7 kt m_b(BGR)=4.1	5.4 kt m_b(BGR)=4.8	14 kt m_b(BGR)=5.1	10 kt m_b(BGR)=5.0	25 kt m_b(BGR)=5.1	< 100 kt m_b(BGR)= 6.1	German Seismic Network
Voytan et al. (2019)	1.4kt (1.2-1.6 kt) depth=430m	5.0 kt (4.7-5.3 kt) depth=600m	13.2 kt (11.9-14.7 kt) depth=430m	11.2 kt (10.6-11.8 kt) depth=710m	18.8 kt (no range) depth=710m	215 kt (200-240 kt) depth=710m	Teleseismic P-wave equalization – pPTime of 1.25 and tunnel grade of 4%
Voytan et al. (2019)	2.3 kt (1.3-3.8 kt) depth=430m	5.5 kt (4.5-6.6 kt) depth=600m	14.3 kt (8.0-23.9 kt) depth=430m	12.5 kt (7.5-19.2 kt) depth=710m	19.7 kt (13.4-28.2 kt) depth=710m	221 kt (148-328 kt) depth=710m	Teleseismic P-wave equalization - 4Hz amplitude absolute modeling
m_b(Lg) Zhao et al (2008; 2012;2014;2016 ;2017; Zhang and Wen, 2013)	0.48 kt m_b(Lg)= 3.93 ± 0.1	7.0 kt ± 1.9 m_b(Lg)= 4.53 ± 0.12	12.2 kt ± 3.8 m_b(Lg)= 4.89 ± 0.14	2-8 kt m_b(Lg) = 4.7 ± 0.2	3-11 kt m_b(Lg) = 4.82±0.2	30-100 kt m_b(Lg) = 5.56±0.2	Depth corrected m_b(Lg)
Full-waveform Yoo (2017); Yoo (2019)	0.8 (0.71-0.85kt) depth= 129m	3.6 (3.3-3.9kt) depth=402m	8.9 (8.6-9.3kt) depth=392m	6.9 (6.3-7.4kt) depth=327m	15.6 (13.4-17.0kt) depth=485m	194.7 (177.2-216.6kt) depth=705m	Full-waveform template matching
Chaves et al. (2018)	-	-	-	-	-	230 kt ±50 m_b=6.3 depth=750m	Teleseismic P-wave stacking

IDC, International Data Centre; NEIC, National Earthquake Information Center; NORSAR, Norwegian Seismic Array BGR, Bundesanstalt für Geowisenschaften; kt, kilotons

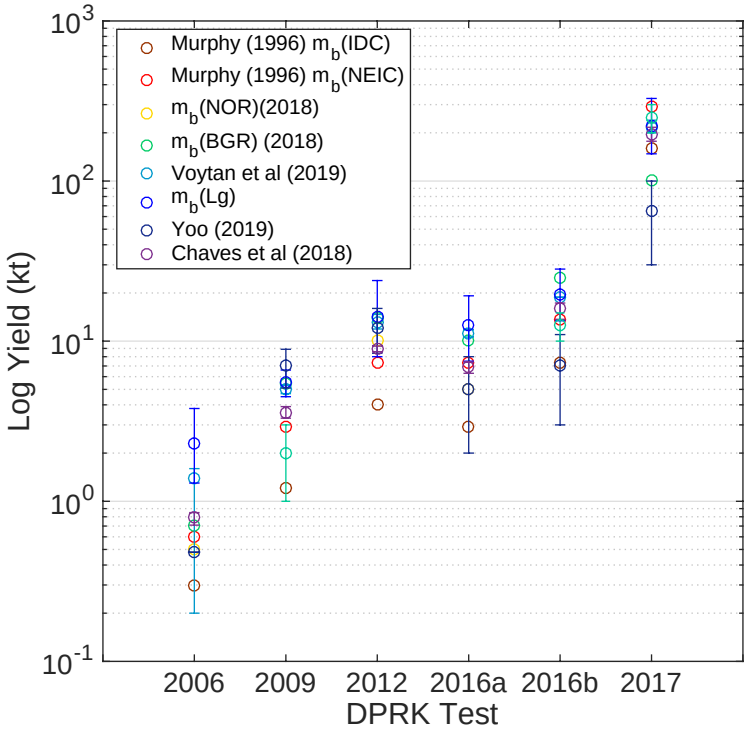

Figure 7. Log yield vs DPRK test by year for the techniques reviewed in Section 3.1 and values listed in Table 3. Range of yield plotted when available.

3.2 Surface-wave Measurements

Surface waves have been used for yield estimation for decades. Similar to a body-wave magnitude, a surface-wave magnitude, *Ms*, can be related to yield. The original method determined *Ms* from 20-sec Rayleigh waves using the formula

$$\boldsymbol{M_s = log\left(\frac{A}{T}\right) + D}, \qquad (10)$$

where *A*, *T*, and *D* are the amplitude in nm, period of the Rayleigh waves in seconds, and a distance-dependent correction term, respectively (Marshall et al., 1979; Bache, 1982; Stevens and Murphy, 2001).

Using surface-wave amplitudes for yield estimation is advantageous because sources show less surface-wave amplitude variation compared to body waves. Bache (1982) states that the network standard deviation of *Ms* is typically half that of m_b. Long-period surface waves are also insensitive to the explosion source function, since the measured period is longer than the explosion source duration (Stevens and Murphy, 2001). Complications in the measurements come from the effects of tectonic strain release and damage and the intricate nature of removing these effects from the amplitudes.

3.2.1 *Long-Period Rayleigh Waves*

Many *Ms*-yield relations have been developed over the years using the basic form $M_s = logY + C$, where Y is the yield in kt and C is a constant that depends on the source material (Murphy, 1997; Marshall et al., 1979; Bache, 1982).

Similar to m_b-yield relationships, multiple sources have derived *Ms*-yield relationships for various size explosions and emplacement conditions. For example, Murphy (1977) found *Ms* = 0.84 log Y+2.14 for explosions less than 100 kt, and *Ms* = 1.33log Y + 1.20 for explosions greater than 100 kt. Relations like these are derived by fitting data with known properties.

Surface-wave yield estimates have developed over the years to account for various emplacement conditions. Stevens and Murphy (2001) tested *Ms*-yield relations for a variety of rock materials. The *Ms* formula used by Stevens and Murphy (2001) is from Rezapour and Pearce (1998), which is based on the International Association of Seismology and Physics of Earth's Interior (IASPEI) *Ms* formula. Stevens' updated formula has an improved distance independence and is based on the theoretical functional form of propagating surface waves from Sato (1967). It is defined as

$$\boldsymbol{M_s = log\frac{A}{T} + \frac{1}{3}log(\Delta) + \frac{1}{2}log(sin(\Delta)) + 0.0046\Delta + 2.370,} \qquad (11)$$

where A is the zero-to peak amplitude in nm, Δ is the distance in degres, and T is the period in seconds. Stevens and Murphy (2001) used long-period *Ms* measurements to constrain a yield relation for various regions of interest with the formula $M_s = \log(Y) + 2.10$ (Figure 8).

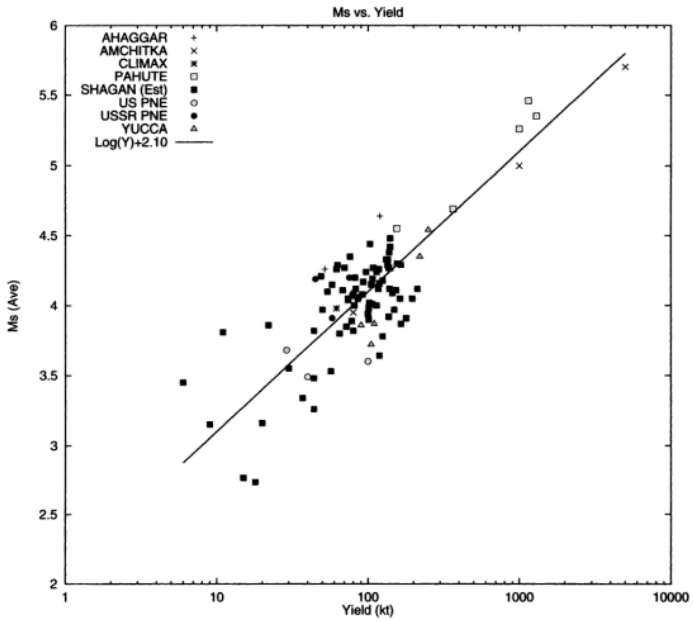

Figure 8. Network-averaged *Ms* vs yield for explosions at various test sites, producing the relation *Ms* = log(Y) + 2.10. From Stevens and Murphy (2001).

One major complication with estimating yield from surface waves is accounting for effects from damage. Long-period surface waves are greatly affected by damage at the source, and the seismic community currently lacks the ability to reliably predict damage (Patton and Taylor, 2011).

3.2.2 *Short-Period Rayleigh Waves*

Short-period fundamental Rayleigh waves, known as Rg, sample a large area of the upper crust as they propagate. This feature makes them are less susceptible than other seismic phases to small scale variations in geologic structures. Estimating yield from event magnitude using Rg (MRg) provides an alternative to estimating yield from direct seismic phases at local and near-regional distances.

Shallow buried and surface explosions generate significant Rg energy at local distances from the source. There are two potential ways to calculate yield from Rg amplitudes: (1) develop an MRg magnitude/yield relation calibrated for above- and below-ground sources, similar to the work of Bonner and Russell (2013) (Figure 9); or (2), directly fit atmospheric and underground synthetics to observed Rg amplitudes (Napoli and Russell, 2018). Bonner and Russell (2013) calculated a MRg-yield relation: MRg = log(Y) – 3.03.

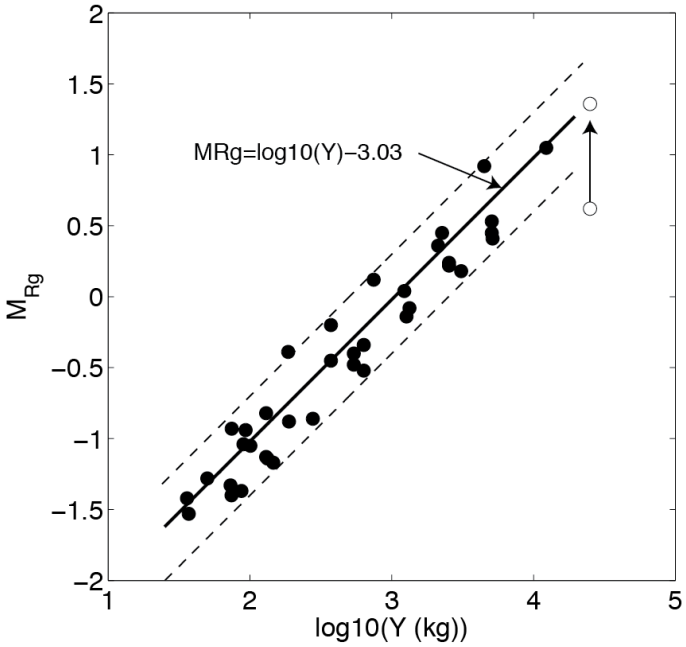

Figure 9. From Bonner and Russell (2013). MRg-yield relation developed from explosion tests in various geologies and areas of interest.

The MRg-yield relation from Bonner and Russell (2013) was only able to account for three types of source geologies, and was unable to account for multiple geologies between the source and receiver. Napoli and Russell (2018) updated the MRg formula from Bonner and Russell (2013) to account for variable geologic media between the source and receiver, thereby extending the use of local Rg measurements for yield estimation to near-regional distances:

$$\boldsymbol{M_{Rg} = log_{10}\left[\frac{u_2(r)}{T_{21}}\right] + log_{10}[C(r)] + log_{10}(e)\gamma_r r,} \qquad (12)$$

where $u_2(r)$ is the Rayleigh displacement corrected for transmission and T_{21} is the frequency

dependent transmission coefficient for a single boundary. $C(r)$ is a distance dependent correction term that accounts for geometric spreading and narrowband filter widths, and γ_r is the path attenuation coefficient. The synthetics and observed Rg displacements should be narrowband filtered sufficiently to remove dispersion and isolate individual frequencies, since T_{21} is frequency dependent (Russell, 2006).

3.2.3 Observations of Surface-Wave Anomalies in the DPRK events

The DPRK nuclear tests exhibited anomalously large *Ms* amplitudes for the m_b values compared to historical nuclear explosions. This caused traditional m_b-*Ms* discrimination methods to improperly screen the DPRK events, as traditional m_b-*Ms* discriminants can fail in an undamaged environment such as North Korea. If the effect of horizontal tectonic release and/or vertical damage is not included, the earthquake and explosion populations may overlap (Kim and Richards, 2007; Bonner et al., 2008, 2011; Koper et al., 2008; Patton and Taylor, 2008; Zhao et al., 2008, 2012; Chun et al., 2011; Napoli et al., 2015). The IDC screening line, defined as $Ms=1.25m_b-2.2$, clearly needed to be revised after DPRK1 and DPRK2 fell on the screening line. While the event screening line does not identify a nuclear explosion, it can indicate that an event is not a nuclear explosion with high probability (Shelby et al., 2012). The revision to the IDC screening line was done to ensure with confidence that any future nuclear explosion is not screened out (Figure 10). In Figure 10 there are m_b and M_s magnitudes for 409 underground nuclear explosions that were used to adjust the IDC screening line to: $M_s=m_b-0.64$. This revised screening line has been in operation at the IDC since June 2010.

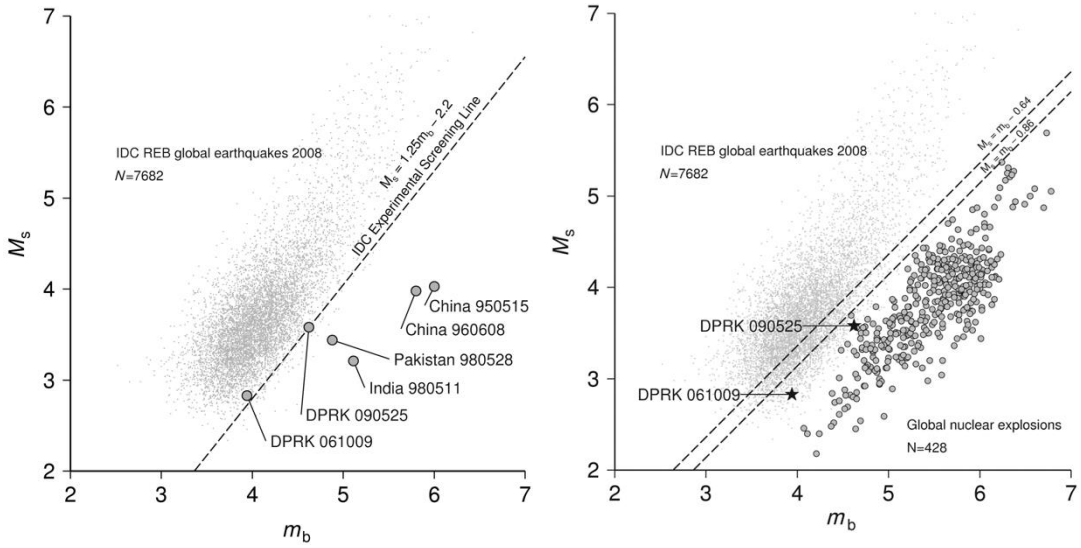

Figure 10. (a) m_b:M_s plot showing the 2008 IDC global event population and the m_b:M_s values for the explosions used in the study by Selby et al. (2012) including DPRK1,2 and other nuclear explosions. (b) Revised m_b:*Ms* plot where the two dashed lines are the bounding line to the explosion population, $Ms = m_b - 0.86$, and the proposed screening line, $Ms = m_b - 0.64$ (From Selby et al., 2012).

Another approach to improving m_b:*Ms* discrimination was proposed by Russell (2006) and Bonner et al. (2006), who developed a variable period surface-wave magnitude, *Ms*(VMAX), which measures surface waves at regional and teleseismic distances. Bonner et al. (2011) enhanced the

Ms(VMAX) method by including Love waves in the magnitude estimation to reduce radiation pattern biasing due to sparse station sampling. Napoli et al. (2015) and Napoli et al. (2017) show that a unified *Ms* measurement, *MsU*, can discriminate the DPRK tests without screening out earthquakes (Figure 11). This discrimination method is further improved by replacing teleseismic m_b with a m_b(P-coda) measurement developed by Yoo (2017) to reduce scattering in m_b results due to sparse station coverage. However, although *MsU* is a reliable discriminant, it is not ideal for yield estimation since it does not account for effects from damage. In addition, using a *MsU* value in a *Ms*/yield relation such as Stevens and Murphy (2001) would overestimate the yield.

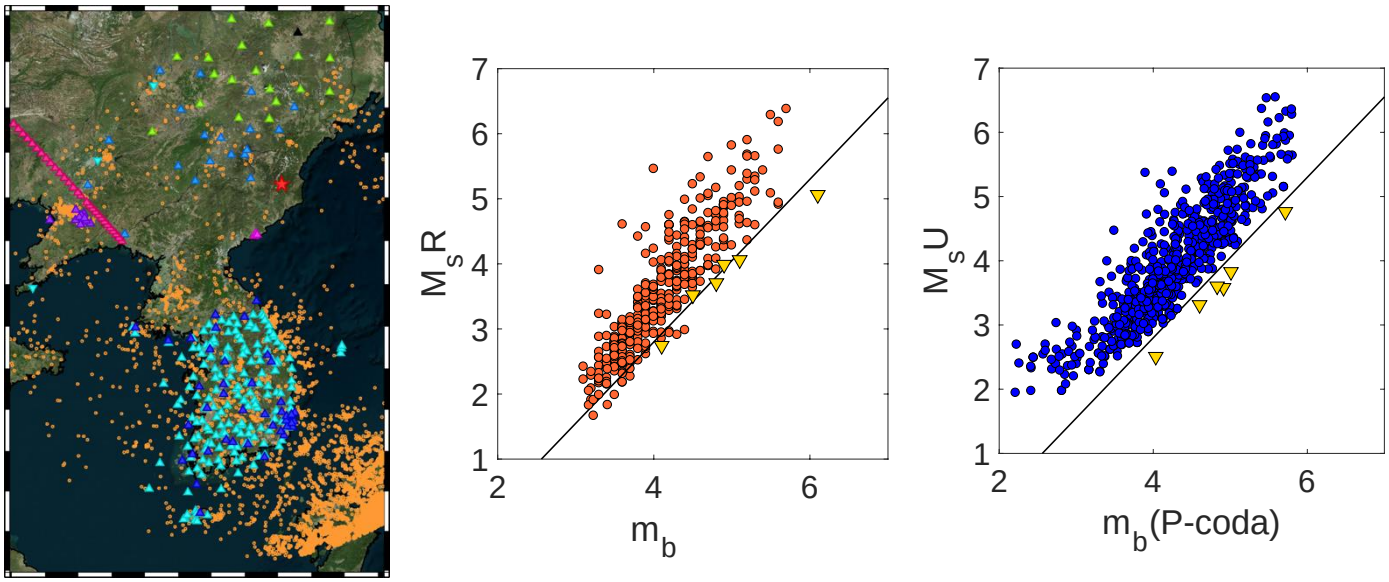

Figure 11. (a) Map of events and stations used in m_b:*Ms* discrimination analysis with red start representing the DPRK test site; (b) MsR vs mb for the Korean dataset where *MsR* is comparable to *Ms*(VMAX) and (c) *MsU* vs m_b(P-coda) which properly identifies all Korean earthquakes and DPRK events (From Napoli et al., 2017).

The nature of the large surface-wave generation by explosions is still a matter of debate in the seismic community, although there are theories related to tectonic strain release (Murphy et al., 2011), damage effects (Patton, 2011), and uncertainties in the transportability of m_b-Ms technologies to new regions. The 3-D nonlinear simulations of Stevens and O'Brien (2018) show that explosions at the base of a mountain can produce amplified surface waves. Using Ms(VMAX) measurements, Stevens and O'Brien (2018) scaled surface-wave amplitudes to relative yields for each DPRK event (see Table 5).

Each method described in this section is summarized below in Table 4 with the references, assumptions, formula, uncertainties and advantages clearly described. Table 5 is a summary of published DPRK yield estimates using each method. Yield estimates for the DPRK tests using *Ms* magnitudes will consistently overestimate yield due to the large surface-wave generation compared to the size of the events. Methods to correct for near-source damage, improve transportability of Ms-yield equations from other regions of interest could improve these

measurements. In Table 5 methods that were not suited for yield estimates, have *Ms* values listed for the DPRK tests.

Table 4. Surface wave techniques, assumptions, uncertainties and advantages

Method	References	Assumptions	Formula	Uncertainties	Advantages
Ms (20 s Rayleigh waves)	Murphy, 1997; Marshall et al., 1979; Bache, 1982	Long period surface wave amplitudes are approx. proportional to yield so the slope of magnitude curve is close to one	Ms = log (Y) + C , where Y is the yield in kt and C is a constant dependent on the source material	Rayleigh wave radiation patterns can introduce biasing with sparse station coverage	Long period surface waves are less susceptible to small scale variations compared to short period body-wave measurements (Bache, 1982).
Ms - distance dependence	Stevens and Murphy (2001); Aduskin (2001); Rezapour and Pearce (1998)	Spall does not contribute to surface waves at longer periods than a few seconds	Updated Ms measurement: $Ms = log\frac{A}{T} + \frac{1}{3}log(\Delta) + \frac{1}{2}\log(\sin(\Delta)) + 0.0046\Delta + 2.370$ Updated Ms-Y relation: *Ms* = 2.10 + 1.0 log W	complicated by tectonic strain release and variations due to near source structure	Updated Ms formula has improved distance independence. Long period surface waves are insensitive to the explosion source function.
MRg	Bonner and Russell (2013); Bonner et al. (2013a)	Assumes that source and receiver are in same geology	MRg = log(Y) - 3.03, where MRg is a 1Hz Rg amplitude measurement that accounts for geometric spreading, attenuation, and excitation	only able to account for three types of geologies, and was unable to account for multiple geologies between the source and receiver; limited to 37 ≤ Y ≤ 12270 kg (TNT equivalent).	At local distances, Rg can be the largest amplitude seismic arrival observed from shallow explosions, mining explosions, and shallow earthquakes
Site-specific MRg	Napoli and Russell (2018)	Prior knowledge of the p-wave velocity and gas filled porosity	This technique is site-specific; the MRg-Y relation changes depending on the location. Example for alluvium earth structure for a fully coupled explosion: MRg= 1.05 log(Y) – 1.72	Height of burst (HOB)/DOB can influence Rg amplitudes and current method only accounts for atmospheric or fully coupled explosions	updated the MRg formula from Bonner and Russell (2013) to account for variable geologic media between the source and receiver, thereby extending distance limitations of MRg

Table 5. Summary of surface wave magnitudes for the DPRK tests

Source	DPRK1	DPRK2	DPRK3	DPRK4	DPRK5	DPRK6	Description
Stevens and O'Brien (2018)	0.91 kt *Ms* =2.90 ± 0.14	4.60 kt *Ms*= 3.61± 0.07	10.0 kt *Ms*=3.95 ± 0.08	12.3 kt *Ms*=4.04 ± 0.04	19.0 kt *Ms* = 4.23 ±0.03	180 kt *Ms*= 5.20 ± 0.05	Ms(VMAX) and scaling yield from DPRK2 published yield from Murphy et al. (2013)
Ms(IDC)	-	M_s(IDC)=3.6	M_s(IDC)=3.9	M_s(IDC)=3.9	M_s(IDC)=4.2	M_s(IDC)=4.9	Reported Ms from the IDC
Napoli et al. (2017)	*MsU*= 2.50	*MsU*=3.31	*MsU*=3.58	*MsU*=3.58	*MsU*=3.82	*MsU*=4.86	Variable period Rayleigh and Love wave Ms based on Bonner et al. (2006); Napoli et al. (2015)
Murphy et al. (2013)	*Ms* =2.93 ± 0.20	*Ms* =3.66 ± 0.10	-	-	-	-	Measured using Ms(VMAX), (Russell, 2006)
Zhao et al. (2017)	*Ms* =2.92 ± 0.20	*Ms*=3.65± 0.07	*Ms*=3.94 ± 0.16	*Ms*=4.05 ± 0.08	*Ms*=4.23 ± 0.09	-	Measured using Ms(VMAX) (Russell, 2006)

3.3 Ground Displacement Measurements

In regions such as North Korea, where deploying seismic sensors is difficult due to political tensions, other non-intrusive methods must be explored to reduce uncertainty in yield estimates. Measuring surface displacements using satellite radar to image the effects from underground nuclear explosions can be used to estimate yield (Wang et al., 2018). Additionally, remote sensing methods can be used to constrain depth and event location. The technology to measure surface displacements with the precision on the order of millimeters has developed in the last 10 years (Adam et al., 2009; Wang et al., 2018), while technology to measure surface displacement from spaceborne interferometric synthetic aperture radar (InSAR) has been around for almost 30 years (Massonnet et al., 1993).

Using InSAR data, it is possible to monitor deformation on the surface after a nuclear test. The first four DPRK tests showed no evidence of measurable surface deformation (Coblentz and Pabian, 2015), and DPRK5 only showed small surface disturbances that were classified as small landslides and possible spall. Although spall is frequently linked to underground nuclear explosions, there is no definitive evidence that DPRK5 caused the surface landslides. DPRK6 was the first North Korean test to produce observable surface deformations directly linked to the underground nuclear test. Pabian and Coblentz (2018) used satellite SAR to identify two zones of slippage/compression on the corner of Mt. Mantap (Figure 12). Contrary to other authors (Wang et al., 2018; Gaebler et al., 2019), Pabian and Coblentz (2018) do not think these subsidence zones can be interpreted as a cavity collapse after DPRK6 since they estimated a deep DOB of 800 m.

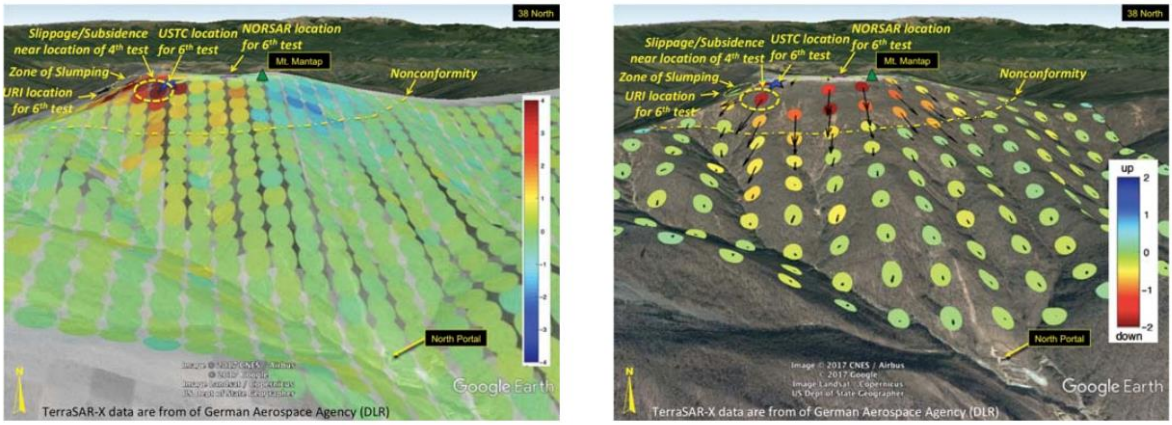

Figure 12. (a) Displacement offsets in meters from DPRK6 overlaid on Google Earth. The color scale represents ground movement along the Line-Of-Sight (LOS) towards the southwest. (b) 3D displacements from DPRK6 with different colors representing vertical movement. Both images were generated using data from TeraSAR-X satellite-based radar from Pabian and Coblentz (2018).

A key factor in reducing uncertainty in ground displacement yield estimations is constraining the depth of the explosion. Sreejith et al. (2019) measured surface deformation using InSAR data and constrained the source characteristics of the nuclear test using Bayesian inversion of the InSAR data (Figure 13). They first constrained the location of the DPRK6 at a depth of ~540 m below Mt. Mantap, and then estimated a yield of 245-271 kt. The authors concluded that the uncertainties in yield and source depth estimated using InSAR data were significantly less than those from seismic data.

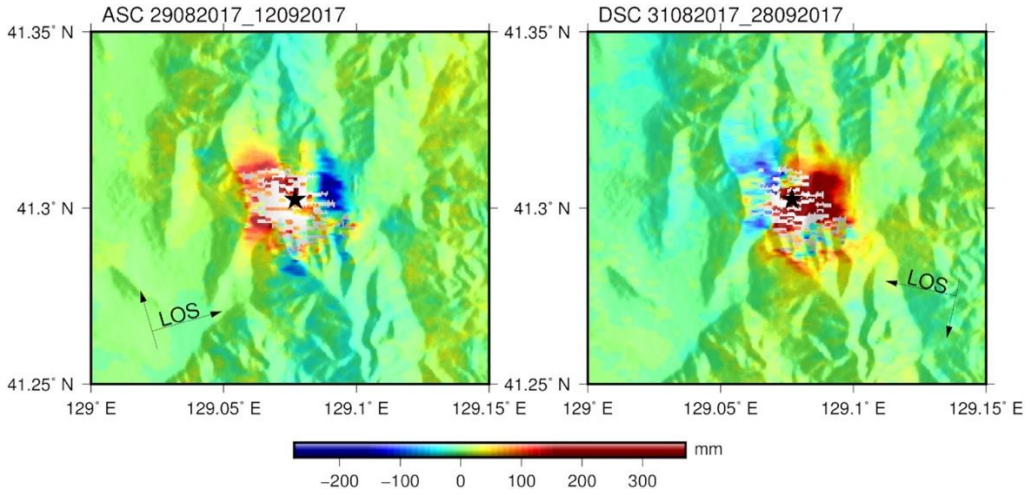

Figure 13. From Sreejith et al. (2019). InSAR data in ascending and descending orbits showing surface deformation associated with the DPRK6.

Wang et al. (2018) applied a similar method to constrain the DPRK6 test to 450 m depth and 191 kt of TNT equivalent, by combining seismic data with surface displacement measured from cross-correlating high resolution spotlight radar images from a German satellite. They were able to

calculate the 3D surface displacements by combining the azimuth and range offsets from two ascending and two descending tracks. The combination of the seismic recordings with the ground displacement data allowed them to reduce their depth uncertainty.

In Table 6 we summarize yield estimation techniques that utilize ground displacement measurements highlighting the references, assumptions, formula, uncertainties and advantages. Table 7 provides the results from ground-displacement studies of the DPRK6 test.

Table 6. Ground displacement yield estimation techniques, assumptions, uncertainties and advantages

Method	References	Assumptions	Formula	Uncertainties	Advantages
Interferometric InSAR	Sreejith et al. (2019)	source model assumes uniform elastic medium and rheological parameters constrained from a limited 1-D seismic velocity model from the Punggye-ri Test Site	Using a Bayesian-based inversion of the InSAR data, determine the source characteristics of the nuclear test (location, depth, yield)	uncertainties in yield and source depth estimated using the Bayesian modelling of InSAR data	Sreejith et al. (2019) concluded that the uncertainties in yield and source depth estimated using the Bayesian modelling of InSAR data are significantly less than those from seismic methods.
Combined seismic and 3D surface displacements	Wang et al. (2018)	assumed a generalized ellipsoidal geometry as there are no known constraints on the geometry of the compaction zone	calculate the 3D surface displacements by combining the azimuth and range offsets from two ascending and two descending tracks	modeling of the geodetic observations reduces the epicentral and depth uncertainties that cannot be resolved solely with seismic	combining seismic data with surface displacement observations

Table 7. Summary of ground displacement yield estimates for DPRK6. We note that there were no observed surface displacements for DPRK1-5.

Source	DPRK6	Notes
Sreejith et al (2019)	245–271 kt depth =542± 30 m	Location for DPRK6 = 129.0769◦E, 41.0324◦N
Wang et al (2018)	191 kt range 171-209kt depth=350-550m	Isotropic seismic moment M=5.05

3.4 Source Spectra

Network averaged P-wave source spectra can be inverted for yield and other source parameters (Murphy, 1989; Murphy et al., 1989). P-wave spectra are unique compared to traditional narrowband magnitude estimators such as m_b and *Ms*, as P-wave spectra can help resolve trade-offs between source and propagation effects in an uncalibrated region (Murphy and Barker, 2001).

Because of this, methods to estimate yield based on P-wave spectra were developed to understand magnitude bias estimates of m_b-yield relations at various nuclear test sites.

A study by Jin et al. (2017) examined seismic spectral ratios between DPRK6 and DPRK2-DPRK5. The magnitude of DPRK1 was too small to produce reliable data for spectral ratios and the location too far from the other events as this method relies heavily on assuming path effects are canceled out in the ratios. Results for the DPRK tests are in Table 9.

Removing path effects along propagation path is complicated, as parameters such as velocity and attenuation models are not always well constrained. To address this problem, Stroujkova (2018) used a nonparametric source spectra inversion method originally from Andrews (1986) that does not require parameterization of the medium along the propagation path. This method estimates the earthquake source spectra as well as the medium transfer functions. Stroujkova (2018) applied this earthquake spectra method to the DPRK nuclear events (Figure 14).

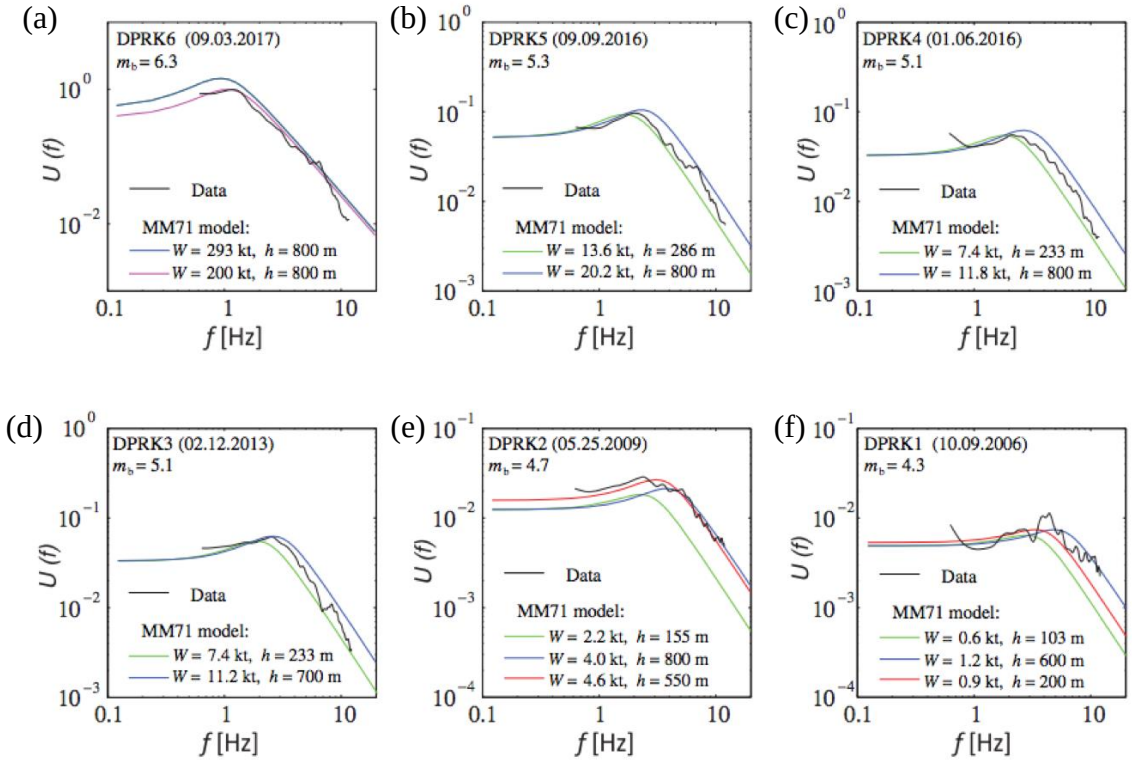

Figure 14. From Stroujkova (2018). P-wave source spectra computed with the MM71 model compared with deconvolved P-wave source spectra for the six DPRK events (a-f). MM71 estimates were made using standard DOB (green), maximum DOB (blue). Red lines represent yield and depth from Murphy et al. (2013). Magenta line in (a) shows the spectrum for DPRK6 predicted from MM71 using a 200-kt yield. Calculated source spectra are in a good agreement with the model-based spectral estimates.

Spectral ratios of events located near each other do have the advantage of canceling out complex path effects; however, questions remain regarding the source characterization (Patton and Taylor, 1995), depth estimation (Murphy et al., 2010, 2013), source scaling (Fisk and Phillips, 2013; Mayeda et al., 2007) and seismic coupling (Stroujkova et al., 2014, 2015) that are necessary to reliably estimate yield (Jin et al., 2017).

3.5 Seismic Moment and Moment Tensor Inversion

Source identification is a crucial step in monitoring analysis, and estimates of seismic moment can help classify the source as an earthquake, explosion, collapse or something more complex. For shallow-depth events, a complicated tradeoff exists between an explosion and a volume-compensated linear-vector dipole (VCLVD), since both sources produce similar intermediate period waveforms at regional distances (Ford et al., 2012). By including teleseismic P waves with the regional approach, confidence in event discrimination can increase, as Ford et al. (2012) proved for the DPRK2 test.

Seismic moment can also be directly tied into yield estimation. Herrmann et al. (2007) and Koper et al. (2008) calculated the seismic moment for DPRK1 from the regional *Rg* waves. Using the isotropic seismic moment, they calculated yield as a function of depth (Figure 15). Their estimates for yield vary between 0.25-2 kt, using a regional velocity model which agrees well with other yield estimates. The yield estimates from Koper et al. (2008) assumed a fully coupled source, which results in a higher potential uncertainty, since the degree of coupling for DPRK1 was not accounted for. In other words, if the DPRK1 test was detonated in an underground cavity, the Koper et al. (2008) yield estimates would underestimate the true yield. The authors noted that seismic amplitudes could be reduced by up to a factor of 70 if the event was fully decoupled.

Seismic moment can also be used to link seismic data from different events recorded at the same station. For instance, Salzberg and Marshall (2007) applied this technique to the DPRK1 test using a Chinese chemical explosion with a known reported yield between 1.2-1.5 tons. By calibrating the recordings from DPRK1 and the Chinese explosion at the Chinese station MDJ using a noise-corrected semi-empirical approach, they estimated the DPRK1 yield to be between 0.37-0.46 kt, which depends on the referenced yield of the Chinese explosion.

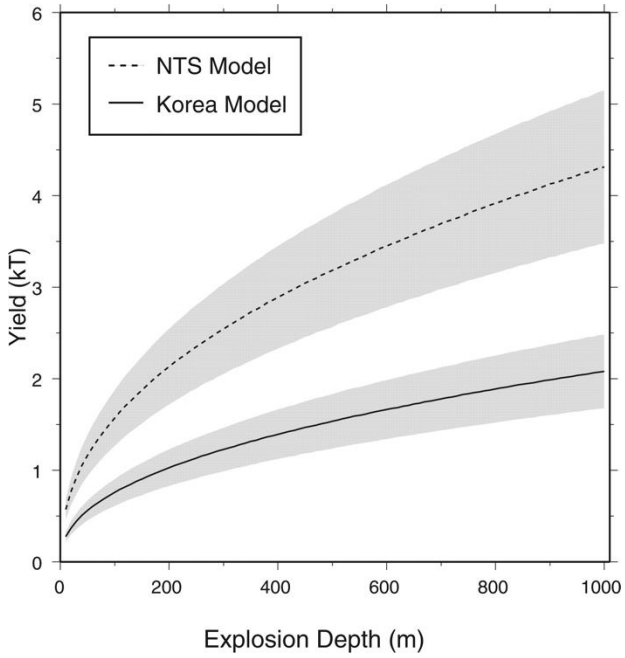

Figure 15. DPRK1 yield estimates (kt) versus explosion depth (m) for an isotropic seismic moment of 3.1(± 0.62) × 10^{21} dyne-cm. The solid line represents a geologic model for the Korean Peninsula and the dashed line corresponds to a geologic model for the Nevada Test Site. The gray shading represents the uncertainty of the standard error of the observed moment (From Koper et al., 2008).

Moment tensor inversions (MTIs) can resolve full moment-tensor components, centroid location and time, as well as constrain uncertainties about the model and source parameters (Gaebler et al., 2019). MTIs have been calculated for all the DPRK explosions (Barth, 2014; Cesca et al., 2017; Ford et al., 2010; Hartmann et al., 2017; Vavryčuk and Kim, 2014; Chiang et al., 2018; Gaebler, et al., 2019).

For example, Gaebler et al. (2019) constrained the best moment tensor for the DPRK6 nuclear test and the aftershock that occurred 8.5 minutes later. For DPRK6, there was a high double-couple (DC) (24%) component found compared to the other DPRK shots, which indicates a difference in near-source damage effects or containment (Barth, 2014; Vavryčuk and Kim, 2014). The best solution has a scalar moment of 2.33×10^{17} Nm (~Mw=5.55) and confirms a shallow depth (400-800m), which agrees with the seismic depth-phase analysis from the same study. For the aftershock, the estimated scalar moment is 1.88×10^{16} Nm (~Mw=4.81). The best-fitting source mechanism indicates a shallow collapse (dominant implosive source component (65%), negative CLVD (29 %), and a DC component (6 %) (Figure 16; from Gaebler et al., 2019).

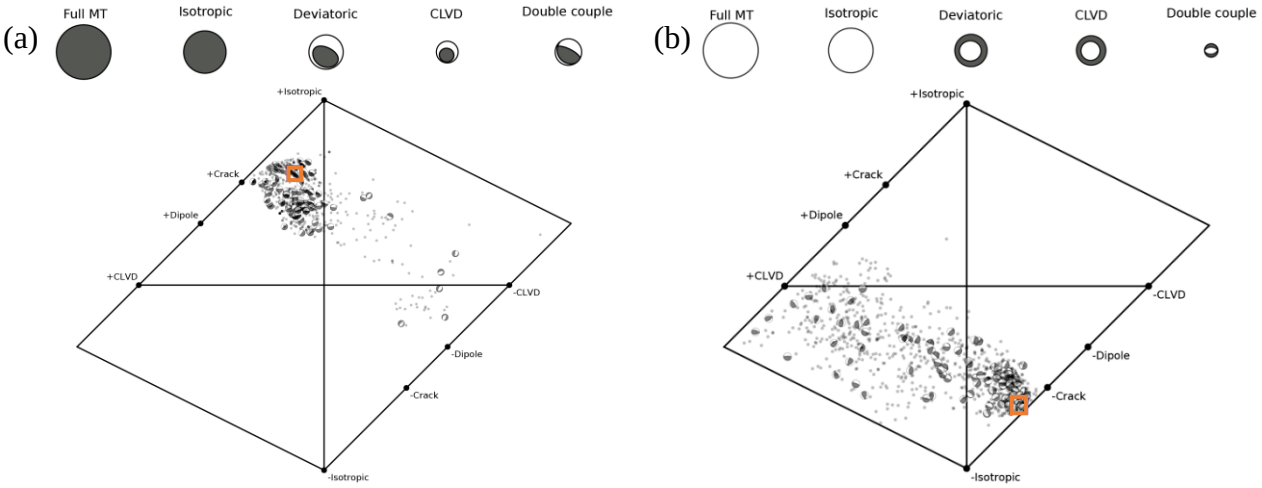

Figure 16. Moment-tensor inversion (MTI) results for DPRK6 and its aftershock. (a) Top: best moment-tensor decomposition, showing the size of the focal spheres scaled with their relative magnitude; bottom: source-type plots demonstrating the best fitting solutions of moment-tensor decomposition with the best solution highlighted in the orange square. (b) Same as in (a), but for the aftershock that occurred 8 minutes after DPRK6 (From Gaebler et al., 2019).

Table 8 summarizes the source-spectra and moment-tensor yield techniques, highlighting the references, assumptions, formula, uncertainties and advantages. Table 9 is a summary of DPRK published yields using these techniques and Figure 17 visualizes the results in Table 9.

Table 8. Source spectra, seismic moment, and MTI yield techniques, assumptions, uncertainties and advantages

Method	References	Assumptions	Description of Method	Uncertainties	Advantages
Source Spectra	Stroujkova (2018)	That the distances of the explosions are short compared to the distance between the test site and the regional stations, so the propagation and the site terms can be combined into a transfer function	Nonparametric inversion method (Andrews, 1986) was used to estimate spectral source signatures	The high-frequency fall-off is proportional to f^{-2}	Does not require parameterization of the medium along the propagation path
Spectral ratios	Jin et al. (2017)	As a first-order approximation, they model teleseismic P as the sum of downgoing P and Pp wave to neglect waves from secondary sources	Spectral ratios calculated for different event pairs from DPRK2-DPRK6 for teleseismic P, regional P and Lg waves	Uncertainty in yield from spectral ratios corresponds to the DOB range from 600-1100m and the uncertainty of the yield is from an assumed uncertainty of +/- 0.1 m.u. in mb from NEIC	Complicated path effects are canceled out while information about the source remains

Seismic Moment	Koper et al. (2008)	Assume a fully coupled source	Estimate seismic moment from regional *Rg*. Using the isotropic seismic moment, calculated yield as a function of depth	Potential for uncertainty due to not accounting for what degree of coupling occurred	The consistency of low-frequency and high-frequency yield estimates argues against significant decoupling for DPRK1
Moment Tensor Inversion	Gaebler et al. (2019)	Full waveforms and their spectra are calculated assuming a layered crustal model proposed by Ford et al. (2010).	Fit low-frequency amplitude spectra and full displacement waveforms in the frequency range from 0.02 to 0.04 Hz (approach by Cesca et al. 2013, 2017)	For the DPRK6 event, the centroid depth is poorly resolved and good waveform fits are found for very shallow sources down to 2.5 km	Resolve full moment tensor components, centroid location and time and constrain uncertainties about the model and source parameters

Table 9. Summary of source spectra yield estimates for DPRK tests

Source	DPRK1	DPRK2	DPRK3	DPRK4	DPRK5	DPRK6	Notes
Stroujkova (2018)	0.6-1.2 depth=200-600m	2.6-4.0 depth=200-800m	7.4-11.2 depth=400-700m	7.4-11.8 depth=600-800m	13.6-20.2 depth=600-800m	150-300 depth=700-800m	Lower bound corresponds to normal DOB and upper bound are for maximum DOB
Koper et al. (2008)	0.25-2kt	-	-	-	-	-	Seismic moment
Salzberg and Marshall (2007)	0.45 kt	-	-	-	-	-	Calibrated recordings from a Chinese explosion
Jin et al., 2017 MM71	-	3-7 kt	6-15 kt	6-15 kt	10-25kt	100-300 kt	Depths range from 600-1,100m; source model MM71
Jin et al., 2017 DJ91	-	0.5-1.5 kt	1.2-3.3 kt	1-3 kt	2-5.4 kt	30-80 kt	Depths range from 600-1,100 m; source model DJ91

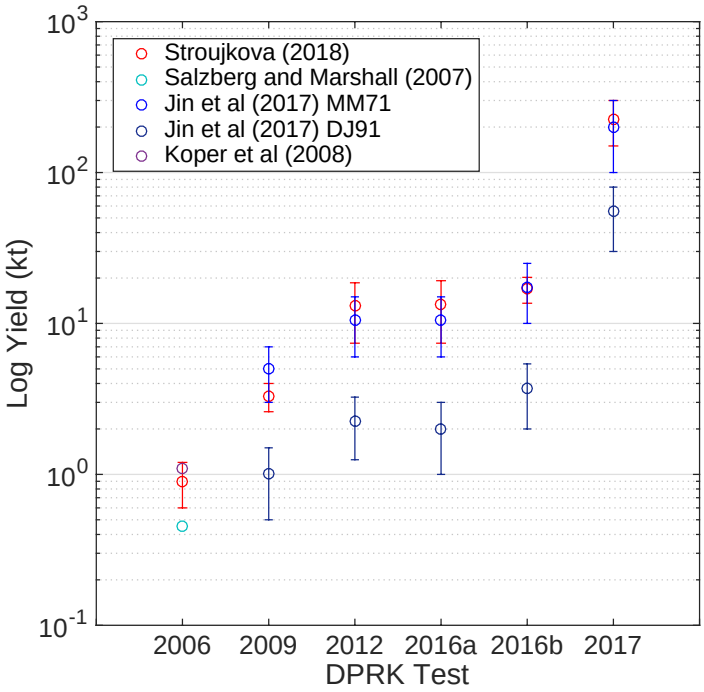

Figure 17. Log yield vs DPRK test by year for the techniques reviewed in Section 3.5 and values listed in Table 9. Range of yield plotted when available.

3.6 Multiple-Method or Coupled Solutions

3.6.1 Coupled Solution of Location, Depth and Yield

Pasyanos and Myers (2018) used a combination of methods to solve the coupled location, depth and yield problem for the DPRK events. To do this, they first calculated event epicentral locations using the software BayesLoc (Myers et al., 2007), which combines arrivals from multiple events to constrain the joint probability of event locations. Then they estimated depth of the tests using topography and tunnel entry points, and finally they used the envelopes of regional signals (Paysanos et al., 2012) to estimate yield (Figure 18). A significant source of uncertainty with this method is the amount of overburden, as it must be well constrained to reduce overall uncertainty. Confidence in the combined solution depends on the quality of the relative locations and the specific explosion source model. Other factors include assumptions about the tunnel properties and the regional propagation characteristics.

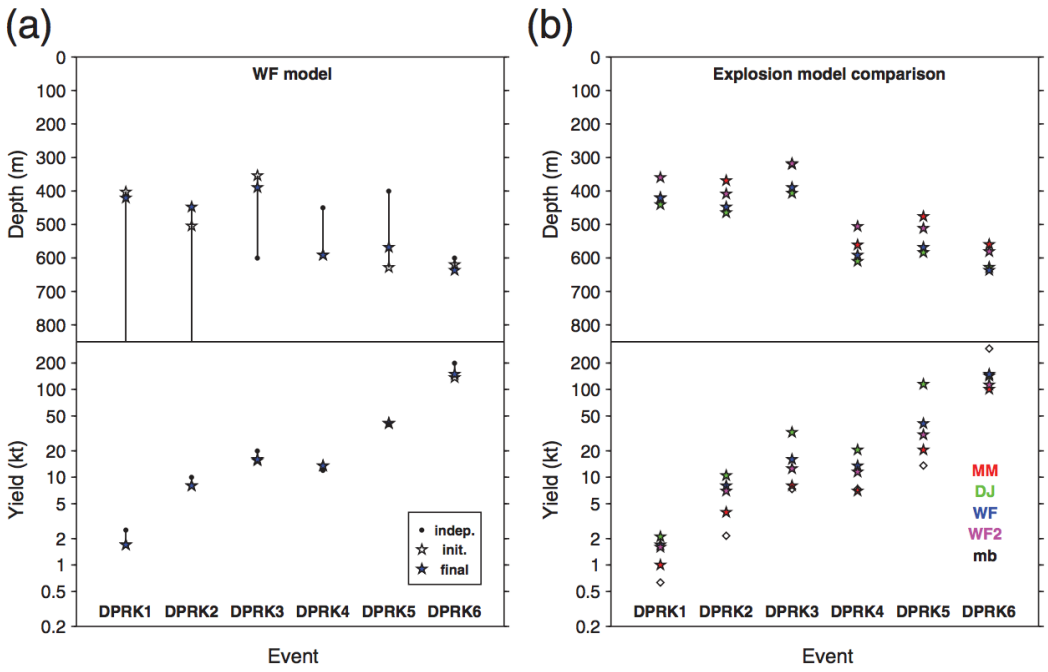

Figure 18. (a) Comparison of depth and yield estimates, where both parameters are independently estimated from envelope misfit for the WF model. (b) Comparison of final estimates for the four source models (MM= Muller and Murphy, 1996; DJ = Denny and Johnson, 1991, WF= Walter and Ford (2018), WF2 = Walter and Ford (2018) modified without the Fisk conjecture) along with m_b-derived yields using the relation from Ringdal et al. (1992) (From Pasyanos and Myers, 2018).

3.6.2 Seismo-Acoustic and Infrasound Signals

Infrasound signals can be generated from underground explosions or earthquakes if ground motions are large enough to produce low-frequency atmospheric waves (Park et al., 2018). These signals decrease with event depth, but when observed they can help discrimination event type and characterize the source since the signals are influenced by depth, yield, and source type (Arrowsmith et al., 2012; Jones et al., 2015; Park et al., 2018). Infrasound signals have traditionally been used to analyze atmospheric explosions, but the DPRK6 test provided the first occurrence of pressure signatures clearly recorded from an underground nuclear test at remote International Monitoring System (IMS) infrasound stations (Gaebler et al., 2019). However, there were additional signals generated from other regions that complicated the signal propagation to remote sensors, which subsequently limited the DPRK6 depth analysis from acoustic signals (Walter and Wen, 2018).

Seismic and acoustic waves provide a natural synergy that can improve knowledge of DOB and yield estimation (Arrowsmith et al., 2010; Bonner et al., 2013b). At some height of burst (HOB) a crossover occurs in which more energy is partitioned as acoustic waves than seismic waves. There are many uncertainties introduced into seismo-acoustic yield estimation including accounting for energy loss due to non-linear effects such as cratering and venting (Bonner et al., 2013b). By quantifying the seismo-acoustic energy partitioning, seismologists can exploit the natural properties of seismic and acoustic waves to calculate the HOB/DOB of an explosion and its yield (Figure 19) (Bonner et al., 2013b; Foxall et al., 2008, 2010; Ford et al., 2014).

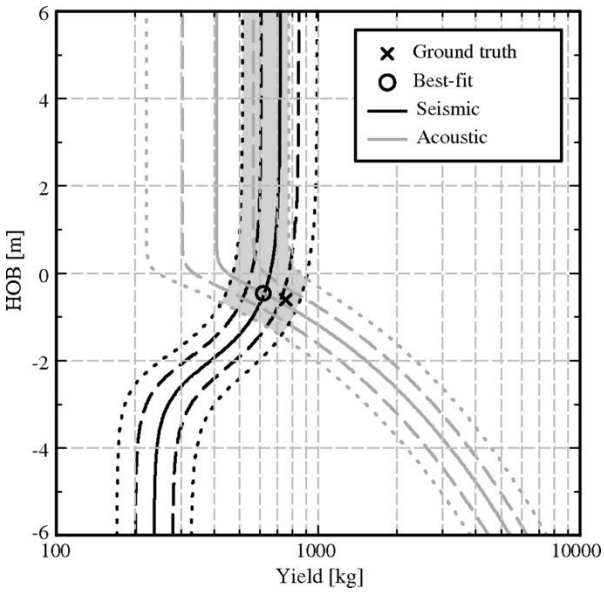

Figure 19. HOB/yield relationship with seismic and acoustic results, highlighting the crossover point at which more energy is partitioned as acoustic waves than seismic waves. This figure from Ford et al. (2014) shows predictions of Humble Redwood 2, shot 4 (HRII-4) at HOB (-0.6), compared with a best-fit solution (circle), which is found via a grid search of the coupled seismic (black line) and acoustic (gray line) models.

A study by Park et al. (2018) investigated estimating yield for DPRK4 and DPRK5 from infrasound signals recorded on seismo-acoustic arrays across South Korea. Origin times of the events were well constrained by seismic data, so infrasound phase identification was based on celerity and phase velocity estimates. Park et al. (2018) calculated yield using empirical relations from Mutschlecner et al. (1999) that relate wind conditions and infrasound amplitudes and the empirical scaling of these relations to high-explosives from Whitaker et al. (2003).

3.6.3 Multi-technologies including seismic and remote sensing

Some of the most promising of the modern yield-estimation techniques fuse data from multiple existing technologies. Gaebler et al. (2019) provides a detailed example of the fusion of multiple techniques to calculate a stable estimation of DPRK6 yield, as well as location, magnitude, and source mechanism. They combined a variety of measurements and analysis techniques, including seismic amplitude measurements, seismic moment calculations, moment-tensor inversion, magnitude and yield estimation, surface displacement measurements, infrasound observations and radionuclide monitoring.

Gaebler et al. (2019) estimated the yield of DPRK6 to be between 160-400 kt. The high upper bound is explained by the enhancement in the P-wave amplitude due to topography and depth phase effects. Section 3.4 of this report noted that DPRK6 exhibited strong surface deformation around the test site (± 10cm), as well as multiple landslides and effects from aftershocks post

detonation. Gaebler et al. (2019) classified the event that occurred 8 minutes after DPRK6 as a cavity collapse. Their conclusion was based on the aftershock's similar depth to DPRK6 and the best moment tensor inversion solution (see Section 3.6). Infrasound signals were measured from both the DPRK6 event and its subsequent aftershock. No radionuclide detection occurred in September, but ^{133}Xe was detected in October, which could possibly be related to delayed leakage from DPRK6. This unique combination of measurements and analyses resulted in reliable estimates of the hypocenter, magnitude, source mechanisms, explosive energy, and potential delayed leakage of ^{133}Xe. Figure 20 summarizes the techniques and results detailed in Gaebler et al. (2019).

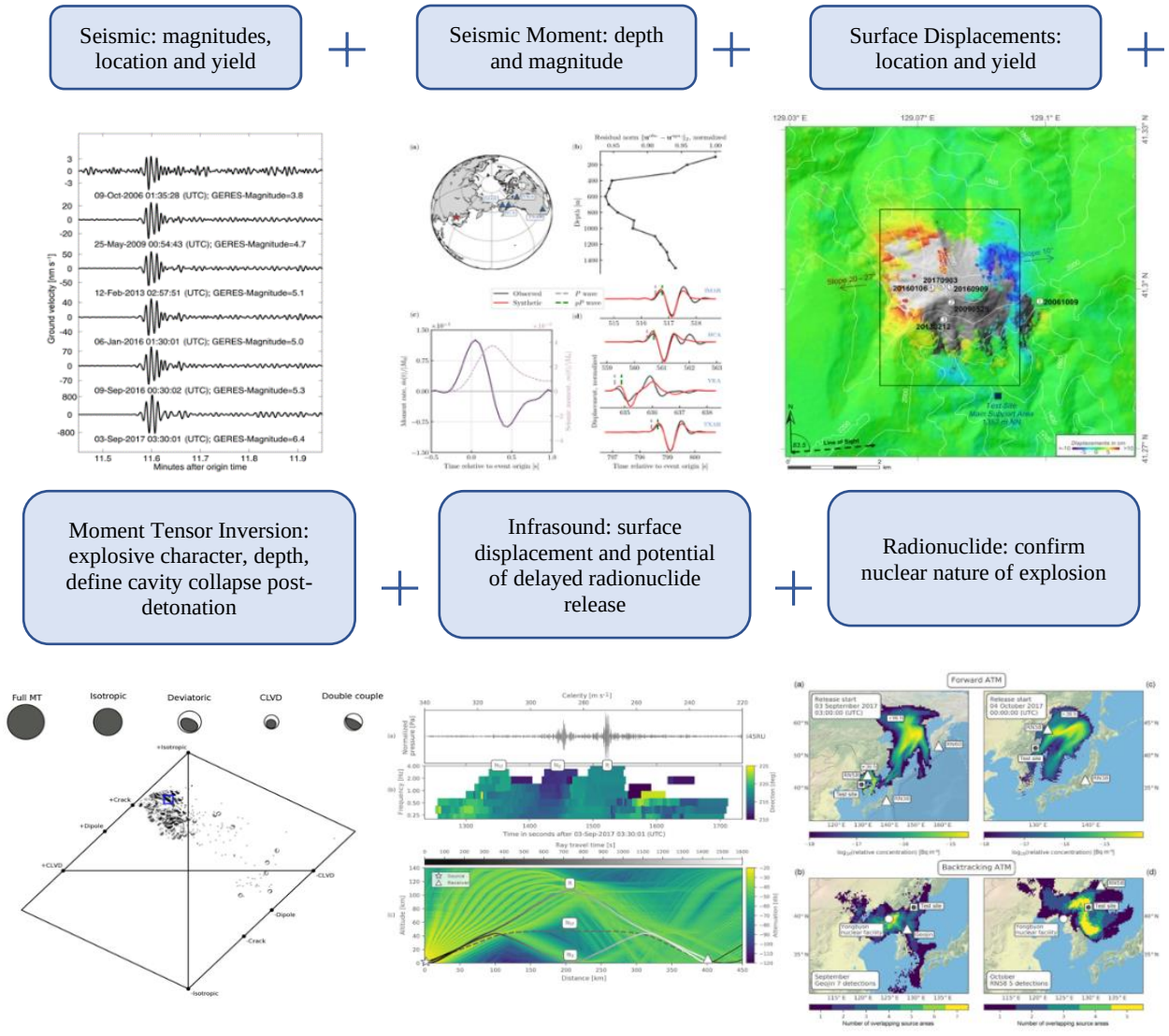

Figure 20. Summary of the multi-phenomenology approach used in Gaebler et al. (2019). This illustration identifies the various techniques used and their respective solution parameters (e.g., depth, magnitude, yield). Please refer to the publication for details on each method and figure component.

Table 10 is a summary of all multi-method techniques, highlighting the references, assumptions, formula, uncertainties and advantages. Table 11 is a summary of DPRK published yields using these techniques and Figure 21 visualizes the results in Table 11.

Table 10. Multi-technology yield estimation techniques, assumptions, uncertainties and advantages

Method	References	Assumptions	Description	Uncertainties	Advantages
Coupled Location/ depth/yield	Pasyanos and Myers (2018)	Because most models to date specify only P-wave explosion source spectra, assumptions need to be made about the S-wave source spectra. Assumptions made about the associated adits and tunnel properties for overburden calculations	first calculate high-precision locations using BayesLoc then estimate depth of the tests using topography and tunnel entry points, finally to estimate yield, they use regional phase coda envelopes using four explosion source models (MM71, DJ91, WF, and WF2).	There remain uncertainties on the relative locations calculated with BayseLoc and there can still be trade-offs between the yield and the depth, leading to uncertainties on both of these parameters.	Help reduce overall trade-offs between location, depth and yield
Infrasound signals on seismo-acoustic arrays	Park et al. (2018)	Assumption that the atmosphere is horizontally stratified and independent of range	Yield estimates are calculated from relating the wind corrected pressure amplitude to the absolute size of the contained explosion, DOB, local material properties, and topography (method derived from Mutschlecner et al. (1999) and Whitaker et al. (2003))	Wind profiles are taken mid-point between the source and receiver but there are associated uncertainties due to stratospheric winds	Use existing seismo-acoustic arrays to measure infrasound signals
seismic/ infrasound/ remote sensing/ moment tensor /radionuclide	Gaebler et al. (2019)	Assumptions are complex as this technique covers multiple technologies. Assumes magnitude–yield relation following Bowers et al. (2001)	Seismic amplitude measurements, seismic moment calculations, moment tensor inversion, magnitude and yield estimation, surface displacement measurements, infrasound observations and radionuclide monitoring all used to estimate various source characteristics, and yield	Multi-technologies with independent or partially independent error structure	The combination of the results from the different technologies and methods yields a reliable estimation of hypocenter, magnitude, explosive energy, source mechanism, and an indication of delayed leakage of ^{133}Xe from the test site.

Table 11. Summary of multi-technology yield estimates for DPRK tests

Source	DPRK1	DPRK2	DPRK3	DPRK4	DPRK5	DPRK6	Description
Pasyanos and Myers, (2018) MM71	1.0 kt depth=420m	4.0 kt depth=369m	8.0 kt depth=320m	7.0 kt depth=561m	20.5 kt depth=476m	101 kt depth=560m	Muller and Murphy (1971) source model
Pasyanos and Myers, (2018) DJ91	2.1 kt depth= 441m	10.5 kt depth=465m	32.5 kt depth=407m	20.5 kt depth=610m	115 kt depth=584m	143 kt depth=628m	Denny and Johnson (1991) source model
Pasyanos and Myers, (2018) WF	1.7 kt depth= 421m	8 kt depth=447m	16.0 kt depth=390m	13.5 kt depth=592m	41.0 kt depth=568m	149 kt depth=636m	Walter and Ford source model
Pasyanos and Myers, (2018) WF2	1.6 kt depth= 360m	7.0 kt depth= 408m	12.5 kt depth=318m	11.5 kt depth= 506m	30.5 kt depth= 511m	113 kt depth= 580m	revised Walter and Ford source model
Gaebler et al., 2019	-	-	-	-		160-400kt	Seismic m_b and Bowers et al., 2018 relation
Park et al., 2018	-	-	-	6.4 kt SD=4.6	-	-	Infrasound signals from seismo-acoustic stations

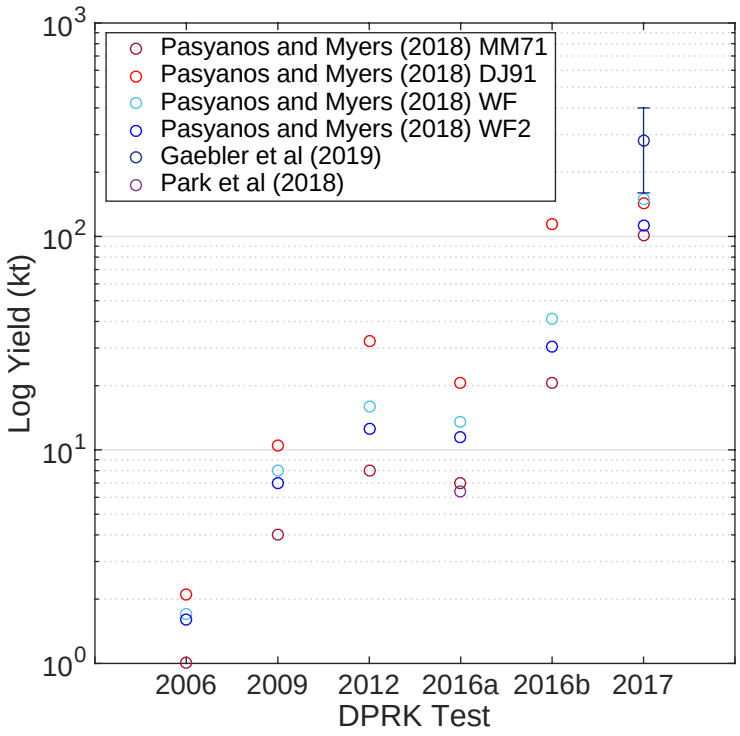

Figure 21. Log yield vs DPRK test by year for the techniques reviewed in Section 3.6 and values listed in Table 11. Range of yield plotted when available.

4. Summary of Yield Method Applications to DPRK Nuclear Tests

While this report highlighted advances in yield estimation over the last 30 years from the OTA (1988), we specifically focused on the difficulties of and advances in yield estimation for the six DPRK underground nuclear tests. Many of the yield techniques discussed in this report have developed out of the necessity of improving yield estimation and discrimination in North Korea. We focused on six main areas of yield estimation in this report as applied to the DPRK tests including (1) body waves, (2) surface waves, (3) ground displacement, (4) source spectra, (5) seismic moment and moment tensor inversion, and (6) multi-technology methods including seismo-acoustic measurements.

Body-wave methods reviewed in this report included traditional teleseismic P-wave techniques (Murphy, 1991; Murphy 1996; Rindgal et al., 1992; Bowers et al., 2001). Various yield estimates applied to the DPRK tests use m_b-yield relations developed for Semipalatinsk and Novaya Zemlya considering the similar hard rock geology and stable tectonic regime to Punggye-ri (Zhao et al., 2012, 2014, 2016; Gaebler et al. 2019). Other modern body-wave techniques included teleseismic P-wave stacking (Chaves et al., 2018), where broadband P waveforms are stacked in azimuthal windows to average path effects and an MM71 source model is used to estimate yield by fitting the waveforms. Teleseismic P-wave equalization presents another approach (Voytan et al., 2019), in which a search over yield and burial depth for a pair of events gives optimal parameters by simultaneous waveform equalization of multiple stations.

Since the original methodology of Nuttli (1973, 1986a), $m_b(Lg)$ methods have advanced to include depth corrections (Zhang and Wen, 2013; Zhao et al., 2012) and an improved RMS amplitude measurement technique to measure *Lg* amplitudes (Schlittenhardt, 2001; Patton and Schlittenhardt, 2005). Yoo's (2017, 2019) full-waveform modeling and coda-derived source calibration methodology sets a new standard for uncertainty analysis, by quantifying uncertainties in measured amplitudes, path propagation and site amplification and incorporating them into a Bayesian yield estimation process.

Surface-wave yield techniques still require improvements to provide stable yield estimates for the DPRK tests, due to the unusually large surface waves produced for the explosion sizes. This caused standard surface-wave yield estimation techniques, such as Stevens and Murphy (2001), to overestimate the yield of the DPRK tests. Methods from Russell (2006), Bonner et al. (2011) and Napoli et al. (2015) aim to stabilize *Ms* measurements by including a variable-period surface-wave measurements for both Love and Rayleigh waves; however, using long-period surface waves for yield estimates without fully understanding how to correct for complicated effects due to damage is unreliable.

The use of ground-surface displacement measurements from satellites has rapidly improved over the last 10 years (Adam et al., 2009), leading to 3D surface measurements and 10-cm resolution today (Wang et al., 2018; Coblentz and Pabian, 2015). These techniques have been specifically useful for the largest magnitude test (DPRK6), since measurable surface displacement was observed that could be attributed to an underground explosion. InSAR data can be used estimate depth, location and yield, and Wang et al. (2018) also included seismic data in their estimates to further resolve the yield. Debate still exists about whether the surface displacements observed from the DPRK6 aftershock were due to cavity collapse (Wang et al., 2018), or if that zone cannot be

interpreted as a collapse/cave-in event (Pabian and Coblentz, 2018). However, the combination of InSAR data and other results from seismic moment tensor inversion indicate that this event can likely be classified as a collapse (Gaebler et al., 2019).

Relative source spectral ratios were useful in estimating yield for DPRK2-DPRK6 due to the proximity of the events. DPRK1 was both too small in magnitude to record high quality seismic data for spectral ratios and the location was further away, which can cause changes in the path effects. Stroujkova (2018) determined that the DPRK source spectra were in good agreement with a MM71 source model and a high-frequency fall-out proportional to f^{-2}. Jin et al. (2017) also estimated spectral ratios for DPRK2-DPRK9 with a MM71 source model with similar results to Stroujkova (2108).

Infrasound signals can be measured on seismo-acoustic arrays (Park et al., 2018) to constrain depth, yield and source type. Seismo-acoustic signals can also be used to can improve knowledge of DOB and yield estimation, because there is a crossover at some HOB at which more energy is partitioned as acoustic waves than seismic waves (Arrowsmith et al., 2010; Bonner et al., 2013b; Ford et al., 2014).

To solve the coupled location, depth and yield problem for the DPRK events, Pasyanos and Myers (2018) first calculated high-precision locations. They then estimated the depth of the tests using topography and tunnel entry points, and then estimated yield from regional-phase coda envelopes using four explosion source models (MM71, DJ91, WF, and WF2). This technique reduces some of the trade-offs between location, depth and yield. The multi-technology approach from Gaebler et al. (2019) is an example of the future direction of yield-estimation methodology, especially in complex environments with many unknowns, such as North Korea. The authors incorporated seven different techniques to resolve location, depth, source characterization, yield and nuclear classification.

Quantifying the uncertainty in each yield estimate is crucial to understanding the physical meaning of the value and to finding ways to improve future analysis techniques. Uncertainty generally comes from either random variation in the measurement or physical variation in the source medium (Vergino and Mensing, 1990). All methods discussed in this report have their uncertainties highlighted in each section, but we note that the largest uncertainties in the DPRK results come from variations in the source model, unconstrained depth/overburden, unknown tunnel geometry, topography effects, ill-constrained source locations, lack of near-source seismic stations and unaccounted-for effects from damage.

Overall uncertainty in a yield measurement can be reduced by either combining multiple technologies that are partially independent, such as various seismic phases, or by having additional information about the test site and emplacement conditions to be able to calibrate yield relations for the area. Using *mb*-Yield relations from NZ and Semipalatinsk is effective; however, the uncertainty could be further reduced if more information about Punggye-ri becomes publicly available in the future. The same improvement could be made with knowledge of velocity structure, or announced emplacement conditions including cavity radius. Although this information currently seems unattainable, in the future DPRK yield estimates would improve with continued resolution of the Punggye-ri test site.

4.1. Focus of Future Yield Estimation Techniques

Yield estimation methods have advanced considerably over the last 30 years. The improvements are wide-ranging and vast: from the use of satellite imagery, to regional and local seismic records, to multi-technology methods, and developments in seismic station instrumentation itself. With time, other enhancements to yield estimation will develop naturally through improvements to sensor hardware and signal propagation theory. In addition, yield estimates will be improved by answering research questions regarding the causes of S-wave generation from explosions and the effects of near-source damage.

From this review of select modern yield techniques focused on the DPRK tests, the most promising methods are the ones that combine multiple methods to constrain various properties of the explosions including location, depth, emplacement conditions and yield. All these factors are connected, and methods aimed at exploiting these connections between technologies will best reduce uncertainty and improve yield estimation. Research could be done to combine many of the techniques described in this report to generate various unified yield techniques. Additionally, if the methods have independent sources of error, the stability of the yield measurement will increase.

Gaebler et al. (2019) represents an excellent example of the future of multi-technology source characterization, location, and yield estimation. By combining several different technologies and analysis techniques, they can constrain depth, source characterization, location and yield. This approach will be crucial in situations where certain yield methods are ineffective due to reasons such as poor signal-to-noise ratios, or signal blockage. A multi-technology approach will be even more effective in circumstances where all technologies can be used simultaneously to constrain important parameters necessary for monitoring purposes.

5. References

Adushkin, V. (2001), Yield Estimation for Semipalatinsk Underground Nuclear Explosions Using Seismic Surface-wave Observations at Near-regional Distances, *Pure appl. geophys.* 158: 2217. https://doi.org/10.1007/PL00001146.

Arrowsmith SJ, Johnson JB, Drob DP, Hedlin MAH (2010) The seismoacoustic wavefield: a new paradigm in studying geophysical phenomena. Rev Geophys 48:RG4003+. https://doi.org/10.1029/2010rg000335

Arrowsmith S.J., Burlacu R., PankowK., StumpB., SteadR., WhitakerR., HaywardC., 2012. A seismoacoustic study of the 2011 January 3 Circleville earthquake, Geophys. J. Int., 189, 1148–1158..10.1111/j.1365-246X.2012.05420.x

Bache, T. (1982). Estimating the yield of underground nuclear explosions, Bull. Seismol. Soc. Am. 72, S131–S168.

Bonner, J. L., D. Russell, D. Harkrider, D. Reiter, and R. Herrmann (2006). Development of a time-domain, variable-period surface wave magni tude measurement procedure for application at regional and teleseismic distances, Part II: Application and Ms–mb performance, Bull. Seismol. Soc. Am. 96, 678–696.

Bonner, J. L., A. Stroujkova, and D. Anderson (2011). Determination of Love- and Rayleigh wave

magnitudes for earthquakes and explosions, Bull. Seismol. Soc. Am. 101, 3096–3104.
Bonner J.L., and D.R. Russell (2013). MRg: A magnitude scale for 1 s Rayleigh waves at local distances with focus on yield estimation. *Bull. Seism. Soc. Am.*, 103, No. 5, 2898-2905.
Bonner, J. L., D. R. Russell, and R. E. Reinke (2013a). Modeling surface waves from aboveground and underground explosions in alluvium and limestone, Bull. Seismol. Soc. Am. 103, no. 6, 2953–2970.
Bonner, J. L., R. Waxler, Y. Gitterman, A. Hofstetter. (2013b). Seismo-Acoustic Energy Partitioning at Near-Source and Local Distances from the 2011 Sayarim Explosions in the Negev Desert, Israel. The Bulletin of the Seismological Society of America. 103. 741-758. 10.1785/0120120181.
Chiang, A., Ichinose, G.A., Dreger, D.S., Ford, S.R., Matzel, E.M., Myers, S.C. & Walter, W.R., 2018. Moment tensor source-type analysis for the Democratic People's Republic of Korea–declared nuclear explosions (2006–2017) and 3 September 2017 collapse event, Seismol. Res. Lett., 89(6), 2152–2165.
Chaves, E. J., Lay, T. & Voytan, D. P. Yield estimate (230 kt) for a Mueller Murphy model of the 3 September 2017, North Korean nuclear test (mbNEIC = 6.3) from teleseismic broadband P waves assuming extensive near-source damage. *Geophysical Research Letters* 45, 10,314–10,322 (2018)
Coblentz, D., & Pabian, F. (2015). Revised Geologic Site Characterization of the North Korean Test Site at Punggye-ri. Science & Global Security, 23(2), 101–120. https://doi.org/10.1080/08929882.2015.1039343
Ford, S. & Dreger, D. & Walter, W. (2010). Source Analysis of the Memorial Day Explosion, Kimchaek, North Korea. Geophysical Research Letters. 12. 15644. 10.1029/2009GL040003.
Ford, S.R. & Walter, W. & Dreger, D. (2012). Event Discrimination using Regional Moment Tensors with Teleseismic-P Constraints. The Bulletin of the Seismological Society of America. 102. 867-872. 10.1785/0120110227.
Ford S.R., A. Rodgers, H. Xu, D. Templeton, P. Harben, W. Foxall, and R. Reinke (2014). Partitioning of seismoacoustic energy and estimation of yield and height-of-burst/depth-of-burial for near-surface explosions, *Bull. Seism. Soc. Am.* 104, 608–623.
Gaebler, P., Ceranna, L., Nooshiri, N., Barth, A., Cesca, S., Frei, M., Grünberg, I., Hartmann, G., Koch, K., Pilger, C., Ross, J. O., and Dahm, T.: A multi-technology analysis of the 2017 North Korean nuclear test, Solid Earth, 10, 59–78, https://doi.org/10.5194/se-10-59-2019, 2019.
Jih. R.-S. and R. A. Wagner (1991). Recent methodological developments in magnitude determination and yield estimation with applications to Semipalatinsk explosions. PL-TR-91-2212(1) (=TGAL91-05), Final Report. Phillips Laboratory. Hanscom Air Force Base. MA.
Jih, R.-S., Wagner, R. A., and R. H. Shumway (1993). Statistical Study of Soviet Nuclear Explosions: Data, Results, and Software Tools. Final Report. Teledyne Geotech Alexandria Laboratory. Alexandria, VA.
Jih, R.-S., and R.R. Baumstark (1994). Maximum-likelihood Network Magnitude Estimates of Low-Yield Underground Nuclear Explosions. Final Report. Teledyne Brown Engineering. Arlington, VA.
Jin, P. H. X., Wang, H., Pan, C., Xu, X., & Wang, X. (2017). Secondary seismic sources behind amplitude ratios between the first 2016 and 2013 North Korean nuclear tests. Geophysical Journal International, 211, 322–334. https://doi.org/10.1093/gji/ggx289
Kim, Won-Young & Richards, Paul. (2007). North Korean Nuclear Test: Seismic Discrimination

at Low Yield. Eos, Transactions American Geophysical Union. 88. 10.1029/2007EO140002.

Kim, K., Rodgers, A., & Seastrand, D. (2018). Local infrasound variability related to in situ atmospheric observation. *Geophysical Research Letters*, 45, 2954– 2962.

Koper, K. D., R. B. Herrmann, and H. M. Benz (2008). Overview of open seismic data from the North Korea event of 9 October 2006, Seism. Res. Lett. 79, 178–185.

Marshall, P. D., D. L. Springer, and H. C. Rodean (1979). Magnitude corrections for attenuation in the upper mantle, Geophys. J. R. Astron. Soc. 57, 609–638.

Mayeda, K. M. and W. R. Walter, (1996). Moment, energy, stress drop and source spectra of Western U.S.earthquakes from regional coda envelopes, *J. Geophys. Res*. 101: 11,195–11,208.

Mayeda, K. & Malagnini, L. & Walter, W. (2007). A new spectral ratio method using narrow band coda envelopes: Evidence for non-self-similarity in the Hector Mine sequence. Geophysical Research Letters - GEOPHYS RES LETT. 34. 10.1029/2007GL030041.

Murphy, J. R., P wave coupling of underground explosions in various geologic media, in Identification of Seismic Sources--Earthquake or Underground Explosion, edited by E. S. Husebye and S. Mykkeltveit, pp. 201-205, D. Reidel, Hingham, Mass., 1981. Newmark, N.M., and W. J. Hall, Earthquake Spectra.

Murphy, J. R. (1996). Types of seismic events and their source descriptions, in Monitoring a Comprehensive Test Ban Treaty, E. S. Husebye and A. M. Dainty editors, Kluwer Academic Publishers, Dordrecht Netherlands, 225-245.

Murphy, J. R., Kitov, I. O., Rimer, N., Adushkin, V. V. and Barker, B. W. 1997. Seismic Characteristics of Cavity Decoupled Explosions in Limestone: An Analysis of Soviet High Explosive Test Data. *Journal of Geophysical Research*, 102(B12): 27393–27405.

Murphy, J.R., and B.W. Barker (2001). Application of network-averaged teleseismic P-wave spectra to seismic yield estimation of underground nuclear explosions. In *Monitoring the Comprehensive Nuclear-Test-Ban Treaty: Source Processes and Explosion Yield Estimation* (pp. 2123-2171). Birkhäuser, Basel.

Murphy, J. R., B. C. Kohl, J. L. Stevens, T. J. Bennett, and H. G. Israelsson (2010), Exploitation of the IMS and other data for a comprehensive, advanced analysis of the North Korean nuclear tests, in 2010 Monitoring Research Review: Ground-Based Nuclear Explosion Monitoring Technologies, pp. 456–465.

Murphy, J. R., Stevens, J. L., Kohl, B. C., Bennett, T. J. (2013). Advanced seismic analyses of the source characteristics of the 2006 and 2009 North Korean nuclear tests, *Bull. Seismol. Soc. Am.*103, 1640–1661, doi: https://doi.org/10.1785/0120120194.

Mutschlecner, J. & Whitaker, Rodney & Auer, Lawrence. (1999). An Empirical Study of Infrasonic Propagation. 10.2172/15133.

Myers, S. C., Johannesson, G., & Hanley, W. (2007). A Bayesian hierarchical method for multiple event seismic location. *Geophysical Journal International*, *171*(3), 1049-1063.

Myers, S.C., Ford, S.R., Mellors, R.J., Baker, S. & Ichinose, G., 2018. Absolute locations of the North Korean nuclear tests based on differential seismic arrival times and InSAR, Seismol. Res. Lett., 89(6), 2049–2058.

Napoli, V.J., Russell, D.R., and Bonner, J. (2015) A Unified Love- and Rayleigh-Wave Magnitude for Improved Discrimination between Earthquakes and Explosions with Application in the Korean Peninsula. *Bull. Seism. Soc. Am.* 105 2235-2241

Napoli, V.J., Yoo, S.H., and D. Russell (2017). Improved mb-Ms discrimination using mb(P-coda) and MsU with application to the six North Korean Nuclear Tests. *American Geophysical Union* Abstract.

Napoli, V.J., and D.R. Russell (2018). Transmission and Reflection of Fundamental Mode Rg Signals from Atmospheric and Underground Explosions. *Bull. Seism. Soc. Am.*; 108 (6): 3590-3597.

Nuttli O. W. (1973). Seismic wave attenuation and magnitude relations for eastern North America, *J. Geophys. Res.* 78, 876- 885.

Nuttli, O. W. (1986a), Yield estimates of nevada test site explosions obtained from seismic *Lg* waves, *J. Geophys. Res.*, 91(B2), 2137– 2151, doi:10.1029/JB091iB02p02137.

Nuttli, O. W. (1986b). Lg magnitudes of selected East Kazakhstan underground explosions, Bull. Seismol. Soc. Am. 76, 1241–1251.

Ringdal, F., P.D. Marshall, and R. W. Alewine (1992). Seismic yield determination of Soviet underground nuclear explosions at the Shagan River test site, *Geophys. J. Int*. 109, 65–77.

Ringdal, F. (1983), Magnitudes from P Coda and Lg Using NORSAR Data, NORSAR Semiannual Technical Summary, 1 Oct 82-31. Mar. 1983, NORSAR Sci. Rep. No. 2-82/83, Kjeller, Norway.

Russell, D. R. (2006). Development of a time-domain, variable-period surface wave magnitude measurement procedure for application at regional and teleseismic distances. Part I—Theory, Bull. Seismol. Soc. Am. 96, 665–677.

Pabian F., Coblentz D., 2018. Observed surface disturbances associated with the DPRK's 3 September 2017 underground nuclear test, Seismol. Res. Lett., 89(6), 2017–2024. 10.1785/0220180120

Park, Junghyun, Il-Young Che, Brian Stump, Chris Hayward, Fransiska Dannemann, SeongJu Jeong, Kevin Kwong, Sarah McComas, Harrison R Oldham, Monique M Scales, Vanshan Wright, Characteristics of infrasound signals from North Korean underground nuclear explosions on 2016 January 6 and September 9, *Geophysical Journal International*, Volume 214, Issue 3, 1 September 2018, Pages 1865–1885, https://doi.org/10.1093/gji/ggy252

Pasyanos, M.E., W.R. Walter, and K.M. Mayeda (2012). Exploiting regional amplitude envelopes: A case study for earthquakes and explosions in the Korean Peninsula, Bull. *Seismol. Soc. Am.* 102, 1938–1948, doi: 10.1785/0120120012.

Pasyanos, M.E., and S. Myers (2018). The Coupled Location/Depth/Yield Problem for North Korea's Declared Nuclear Tests. *Seismol. Res. Ltrs*. 89. doi: 10.1785/0220180109.

Patton, H. J. (1988). Application of Nuttli's method to estimate yield of Nevada test site explosions recorded on Lawrence Livermore National Laboratory's digital seismic system, Bull. Seismol. Soc. Am. 78, 1759–1772.

Patton, H.J. (2001), *Network m_b(Lg) calibration for stations in central Asia, Technical Report No. LA-CP-01-0375*, Los Alamos National Laboratory, University of California, p. 29.

Patton, H. J., and J. Schlittenhardt (2005), A transportable m_b(*Lg*) scale for central Europe and implications for low-magnitude M_s-m_b discrimination, *Geophysical Journal International*, 163(1), 126–140, https://doi.org/10.1111/j.1365-246X.2005.02663.x

Patton, H. J., and S. R. Taylor (2011), The apparent explosion moment: Inferences of volumetric moment due to source medium damage by underground nuclear explosions, J. Geophys. Res., 116, B03310, doi:10.1029/2010JB007937.

Patton, H. J. (2013), Analysis of mb-Ms Relationships for Stable and Tectonic Test Sites:

Implications for Source Discrimination and Yield Estimation of North Korean Tests. *Los Alamos National Laboratory Report LA-UR-13-21964*

Phillips, W. S. and X. Yang (2017) SPE Source spectral ratios. Technical Report, LA-UR-17 21715, doi: https://doi.org/10.2172/1345906.

Priestley K.F. and Patton H.J., 1997. Calibration of m_b(*Pn*), m_b(*Lg*) scales and transportability of the M_o: m_b discriminant to new tectonic regions, *Bull. seism. Soc. Am.*, 87, 1083–1099.

Rezapour, M. and Pearce, R.G. (1998), Bias in Surface-wave Magnitude Ms due to Inadequate Corrections, Bull. Seismol Soc. Am. 135-138.

Schlittenhardt, J. (2001). Teleseismic Lg of Semipalatinsk and Novaya Zemlya nuclear explosions recorded at the GRF (Gräfenberg) array: comparison with regional Lg (BRV) and their potential for accurate yield estimation, Pure Appl. Geophys. 158, 2253–2274.

Selby, N. D., P. D. Marshall, and D. Bowers (2012). mb:Ms event screening revisited, Bull. Seismol. Soc. Am. 102, 88–97.

Stevens, J. L., and S. M. Day (1985). The physical basis of the mb:MS and variable frequency magnitude methods for earthquake/explosion discrimination, J. Geophys. Res. 90, 3009–3020.

Stevens, J. L., and K. L. McLaughlin (2001). Optimization of surface wave identification and measurement, in Monitoring the Comprehensive Nuclear Test Ban Treaty: Surface Waves, A. Levshins and M. H. Ritzwoller (Editors), Pure Appl. Geophys. 158, 1547–1582.

Stevens, Jeffry & Murphy, John. (2001). Yield Estimation from Surface-wave Amplitudes. Pure and Applied Geophysics. 158. 2227-2251. 10.1007/PL00001147.

Stevens, J.L., and O'Brien, M. "Seismic wave generation and propagation from complex 3D explosion sources," in *Proceedings of the 33th Monitoring Research Review: Ground-Based Nuclear Explosion Monitoring Technologies*, pp. 582–591, Tucson, Ariz, USA, September 2011.

Sreejith, K.M., Ritesh Agrawal, A S Rajawat, Constraints on the location, depth and yield of the 2017 September 3 North Korean nuclear test from InSAR measurements and modelling, *Geophysical Journal International*, Volume 220, Issue 1, January 2020, Pages 345–351.

Stroujkova, A., Reinke, R., Duray, J., & Bonner, J. (2014). Cavity decoupling of small explosions in limestone. Bulletin of the Seismological Society of America, 104(3), 1205–1211. https://doi.org/10.1785/0120130206

Stroujkova, A., Leidig, M., & Bonner, J. (2015). Effect of the detonation velocity of explosives on seismic radiation. Bulletin of the Seismological Society of America, 105(2A), 599–611. https://doi.org/10.1785/0120140115

Stroujkova, A. (2018). Extracting the source spectra for the North Korean nuclear tests. Seismological Research Letters, 89(6), 2174–2182. https://doi.org/10.1785/0220180125

U.S. Congress, Office of Technology Assessment, *Seismic Verification of Nuclear Testing Treaties*, OTA-ISC-361 (Washington, DCL U.S. Government Printing Office, May 1988).

Vergino, Eileen S., and Richard W. Mensing. Yield estimation using regional m_b(*Pn*). *Bulletin of the Seismological Society of America* ; 80 (3): 656–674.

Voytan, D. P., Lay, T., Chaves, E. J., and Ohman, J.T. (2019). Yield Estimates for the Six North Korean Nuclear Tests From Teleseismic *P* Wave Modeling and Intercorrelation of *P* and *Pn* Recordings. *Journal of Geophysical Research: Solid Earth, 124.* https://doi.org/10.1029/2019JB017418

Walter, William R., and Wen, Lianxing. Preface to the Focus Section on North Korea's September

2017 Nuclear Test and Its Aftermath. United States: N. p., 2018. Web. doi:10.1785/0220180281

Walter, William R., Douglas A. Dodge, Gene Ichinose, Stephen C. Myers, Michael E. Pasyanos, Sean R. Ford (2018). Body-Wave Methods of Distinguishing between Explosions, Collapses, and Earthquakes: Application to Recent Events in North Korea. *Seismological Research Letters*; 89 (6): 2131–2138.

Walter W. R., and Ford, S. R.2018. A preliminary explosion seismic spectral model for saturated/hard rock, *Tech. Rept. LLNL-TR-754292*, Lawrence Livermore National Laboratory, Livermore, California, 14 pp.

Wang, T., Shi, Q., Nikkhoo, M., Wei, S., Barbot, S., Dreger, D., *et al*. (2018). The rise, collapse, and compaction of Mt. Mantap from the 3 September 2017 North Korean nuclear test. *Science*, 361(6398), 166-170. doi: 10.1126/science.aar7230.

Yoo, S.-H. (2017). Stable and transportable seismic yield estimation from local full-envelope template matching. *Bulletin of the Seismological Society of America*, *107*(2), 660–673. https://doi.org/10.1785/0120150148

Yoo, S.-H. (2019). Application of Advanced Numerical Techniques to Improve the Estimation of Explosion Yield and Quantify Its Uncertainty. Seismological Society of America. *Abstract*.

Zhang, M. & Wen, L.X., 2013. High-precision location and yield of North Korea's 2013 nuclear test, Geophys. Res. Lett., 40, 2941–2946.

Zhao, L.F., Xie, X.B., Wang, W.M. & Yao, Z.X., 2008. Regional seismic characteristics of the 9 October 2006 North Korean nuclear test, Bull. seism. Soc. Am., 98, 2571–2589.

Zhao, L.F., Xie, X.B., Wang, W.M., Zhang, J.H. & Yao, Z.X., 2010. Seismic Lg-wave Q tomography in and around Northeast China, J. geophys. Res., 115, B08307, doi:10.1029/2009JB007157.

Zhao, L.F., Xie, X.B., Wang, W.M. & Yao, Z.X., 2012. Yield estimation of the 25 May 2009 North Korean nuclear explosion, Bull. seism. Soc. Am., 102, 467–478.

Zhao, L.F., Xie, X.B., Wang, W.M. & Yao, Z.X., 2014. The 12 February 2013 North Korean underground nuclear test, Seismol. Res. Lett., 85, 130–134.

Zhao, L.-F., Xie, X.-B., Wang, W.-M., Hao, J.-L. & Yao, Z.-X., 2016. Seismological investigation of the 2016 January 6 North Korean underground nuclear test, Geophys. J. Int., 206(3), 1487–1491.